AD-A190 206 STUDY OF MEAN FREE PATH EFFECTS ON GROWTH OF ULTRAFINE METALLIC AEROSOLS..(U) RESEARCH TRIANGLE INST RESEARCH TRIANGLE PARK NC P A LAWLESS NOV 87 AFOSR-TR-87-1740 1/1

UNCLASSIFIED F49620-84-C-0017 F/G 4/1 NL

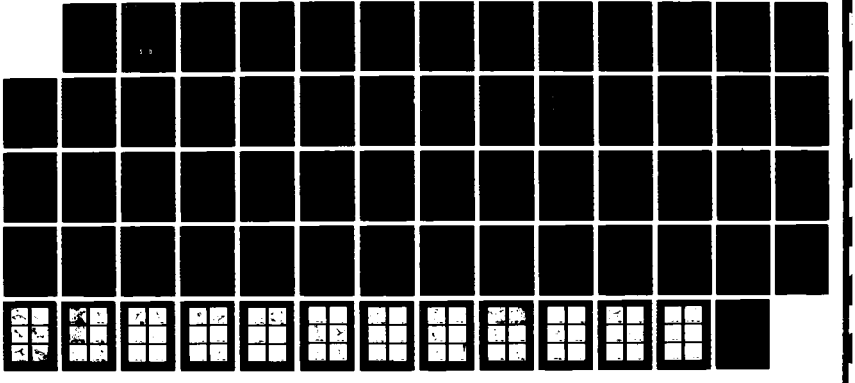

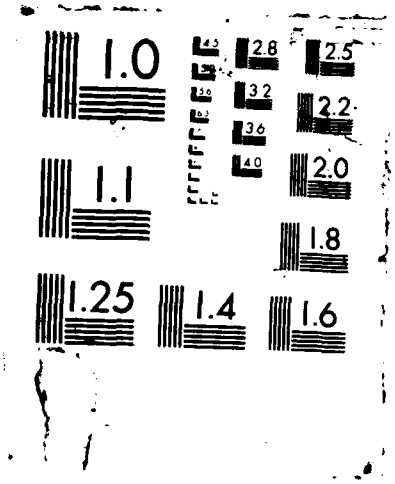
1.0
2.8
2.5
3.2
2.2
3.6
4.0
2.0
1.1
1.8
1.25
1.4
1.6

(2)

AFOSR-TR- 87-1740

RESEARCH TRIANGLE INSTITUTE

November 1987

Study of Mean Free Path Effects on Growth of Ultrafine Metallic Aerosols

Final Report

Work performed under
AFOSR Contract Number F49620-84-C-0017

Prepared for
Air Force Office of Scientific Research
Bolling Air Force Base
Washington, DC

Prepared by
Research Triangle Institute
P.O. Box 12194
Research Triangle Park, NC 27709

Principal Investigator
Dr. Philip A. Lawless

POST OFFICE BOX 12194 RESEARCH TRIANGLE PARK, NORTH CAROLINA 27709

SECURITY CLASSIFICATION OF THIS PAGE

REPORT DOCUMENTATION PAGE

1a. REPORT SECURITY CLASSIFICATION UNCLASSIFIED	1b. RESTRICTIVE MARKINGS
2a. SECURITY CLASSIFICATION AUTHORITY	3. DISTRIBUTION / AVAILABILITY OF REPORT Approved for public release; distribution unlimited.
2b. DECLASSIFICATION / DOWNGRADING SCHEDULE	
4. PERFORMING ORGANIZATION REPORT NUMBER(S)	5. MONITORING ORGANIZATION REPORT NUMBER(S)
6a. NAME OF PERFORMING ORGANIZATION: Research Triangle Institute 6b. OFFICE SYMBOL (If applicable): CAT	7a. NAME OF MONITORING ORGANIZATION: Air Force Office of Scientific Research AFOSR-TR-87-1740
6c. ADDRESS (City, State, and ZIP Code): P.O. Box 12194 Research Triangle Park, NC 27709	7b. ADDRESS (City, State, and ZIP Code): Building 410 Bolling AFB, DC 20332
8a. NAME OF FUNDING / SPONSORING ORGANIZATION: Same as 7a 8b. OFFICE SYMBOL (If applicable): NE	9. PROCUREMENT INSTRUMENT IDENTIFICATION NUMBER: F49620-84-C-0017
8c. ADDRESS (City, State, and ZIP Code): Same as 7b	10. SOURCE OF FUNDING NUMBERS PROGRAM ELEMENT NO.: 61102F PROJECT NO.: 2306 TASK NO.: C4 WORK UNIT ACCESSION NO.

11. TITLE (Include Security Classification)
Study of Mean Free Path Effects on Growth of Ultrafine Metallic Aerosols (Unclassified)

12. PERSONAL AUTHOR(S)
Lawless, Philip Austin

13a. TYPE OF REPORT	13b. TIME COVERED	14. DATE OF REPORT (Year, Month, Day)	15. PAGE COUNT
Final	FROM 86 July TO 87 Sept	87 Nov 31	65

16. SUPPLEMENTARY NOTATION

17. COSATI CODES		
FIELD	GROUP	SUB-GROUP

18. SUBJECT TERMS (Continue on reverse if necessary and identify by block number)
Aerosols, metallic aerosols, growth of aerosols, mean free path, reduced pressure, exoatmospheric

19. ABSTRACT (Continue on reverse if necessary and identify by block number)

This is the final report of activities on a study of metallic aerosol growth under reduced pressure conditions. The aerosol produced is very complex in shape, and the use of fractal descriptors was investigated. The report details the kind of fractal analysis used. It shows that the particles have fractal characteristics that describe stages of growth and that the pressure under which the particles are grown does influence the growth structure. At very low pressures, the particles fail to form because of chamber size limitations. The conclusions reached in the report show some of the utility of fractal analysis for investigating irregular particle shapes, some of the pressure effects on formation of metallic aerosols of different compositions, and extrapolations of the growth conditions to lower pressures.

20. DISTRIBUTION / AVAILABILITY OF ABSTRACT ☐ UNCLASSIFIED/UNLIMITED ☐ SAME AS RPT. ☐ DTIC USERS	21. ABSTRACT SECURITY CLASSIFICATION
22a. NAME OF RESPONSIBLE INDIVIDUAL: Dr. Alan Rosenstein	22b. TELEPHONE (Include Area Code): (202) 767-4953 22c. OFFICE SYMBOL: NC

DD FORM 1473, 84 MAR 83 APR edition may be used until exhausted. All other editions are obsolete.

SECURITY CLASSIFICATION OF THIS PAGE

UNCLASSIFIED

Study of Mean Free Path Effects on Growth of Ultrafine Metallic Aerosols

Final Report

by

P. A. Lawless
Research Triangle Institute
Research Triangle Park, NC 27709

and

P. C. Reist
University of North Carolina
Chapel Hill, NC 27514

AFOSR Contract Number F49620-84-C-0017

November 1987

CONTENTS

FIGURES

TABLES

1.0 INTRODUCTION

This is the final report on a project for investigating the dynamics of aerosol formation in gaseous atmospheres ranging from conditions at the Earth's surface to those in the extreme upper atmosphere. The research involves theoretical and experimental determination of the behavior of ultrafine aerosol particles at high concentrations. The normal diffusion-limited coagulation and growth of aerosols is expected to be strongly modified as the particle diameter and the interparticle separation approach the mean free path of the gas molecules.

In the first year, the experimental facility was set up, using an exploding wire generator for the production of high concentrations of metallic aerosols. The experiments were devoted to development of sampling methods for the reduced atmosphere environment, and then to the observation of the types of behavior exhibited by single component aerosols. The types of aerosols generated were highly irregular in appearance, consisting of branched chains of small, spherical particles. The irregular appearance led us to consider the application of fractal mathematics for describing the particles and the physical processes behind their growth.

Much of the second year's efforts were devoted to the fractal analysis of the aerosols and the interpretation of the results. Fractal analysis is still in an embryonic state with regard to applications in physical measurements, and the techniques used in one situation may not be the best to use in another. The investigation of techniques for measuring fractal dimensions led us to reject several methods as inapplicable to the problem of characterizing aerosol particles and to refine the use of others to obtain consistency among methods. The correlation and circular dilation techniques have been the methods of choice in analyzing micrographs of the aerosol particles. These methods also belong to the same category of analytical techniques used in theoretical models of particle growth processes, which allows us to compare the experimental measurements with model results.

In the third year's work, emphasis was placed on answering the questions raised in the experiments and analysis of the prior work. Theoretical test particles were developed to challenge the analytical techniques. Ensembles of real particles were measured to obtain the statistical properties of the fractal dimensions for aerosols grown under identical conditions. Several new materials were used for the aerosol source material to determine what differences of growth could be expected and what other effects, such as electrical charging, would be encountered.

This report summarizes the work of the prior years and explains in detail the work carried on in this last year's effort.

2.0 SUMMARY OF PRIOR WORK

2.1 YEAR ONE

Most of the first year's effort was devoted to setting up the experimental apparatus for generating and growing aerosols at reduced pressures. While this was being done, theoretical studies were undertaken of the kinds of growth that could be expected.

2.1.1 Theoretical Work

The condensation of a saturated vapor into a liquid phase of droplets produces a quite monodisperse aerosol when the growth is diffusion-limited. Subsequent growth of the aerosol as a liquid follows general patterns. In the continuum regime, particle diameters $\gg$ the gas mean free path, the particle size distribution evolves toward a steady shape that is fairly broad. In the free-molecular regime, particle diameters $\ll$ the gas mean free path, the size distribution evolves toward a similar but distinct shape. As a result of a study of the growth of liquid droplets in the transition regime, between the free-molecular and continuum regimes, a third size distribution was determined that is significantly narrower than the other two, as shown in Figure 1.

This transition distribution is a transient distribution that will eventually grow into the continuum regime distribution; however, for a wide range of initial particle sizes and concentrations, the size distribution changes so slowly with time that it can be considered quasistatic.

When the liquid aerosol is a molten metal that eventually solidifies, the frozen droplets may then continue to collide and stick to one another, but they will maintain the shape and diameter they had at the time of freezing. This fact makes an analysis of the diameters feasible, even after the primary particles have been incorporated into quite complex particle agglomerates. This will be taken up in the discussion of the third year's work.

Although condensation and growth of aerosols in the liquid state were given a theoretical treatment in the first year [1], the observations of the

Steady-State Distributions for Atmospheric Pressure

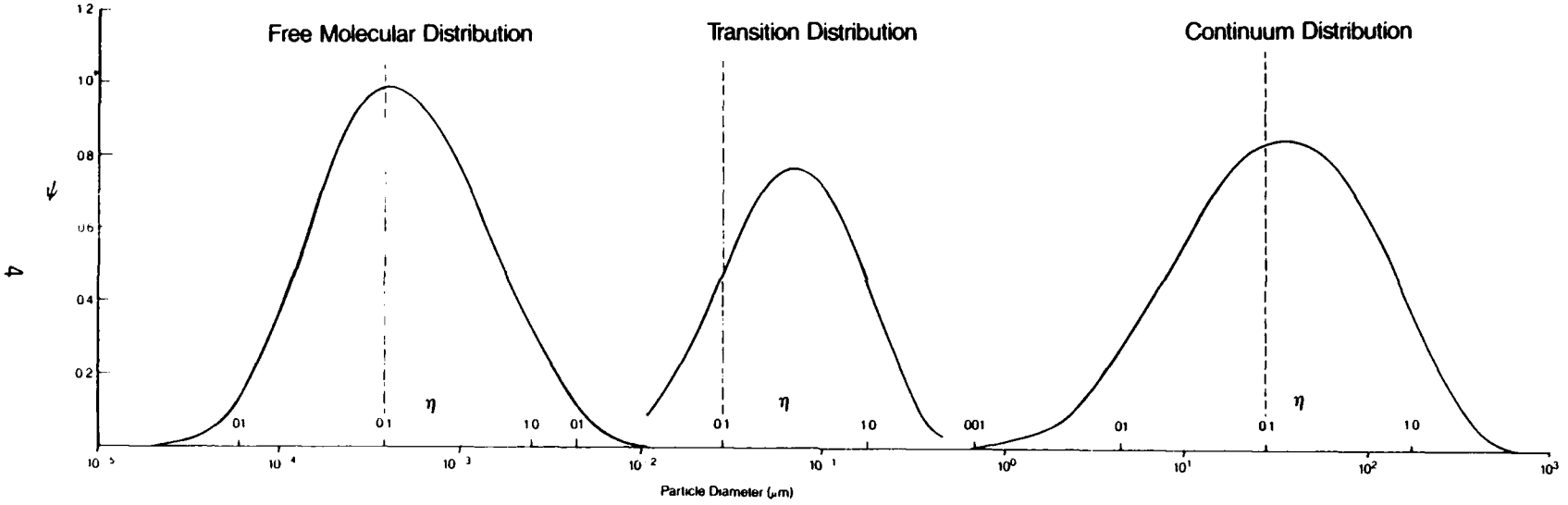

Figure 1. Three regimes for particle growth and their characteristic distributions.

experimental particles quickly showed that the solid particle growth was much more complex than could be treated with the standard theoretical methods.

2.1.2 Experimental Work

The aerosol was produced with an exploding wire generator (EWG) [1] on which was mounted a 0.1 m^3 growth chamber capable of being evacuated to 10 to 4 atm or below. The aerosol was removed from the chamber for capture on a filter or analysis in an optical particle counter (OPC) by capturing it in a small (145 cm^3) internal chamber that was then raised to atmospheric pressure and flushed.

The chamber technique worked satisfactorily at all pressures. At low pressures, the aerosol particles settled completely in about 0.5 h, but at 1.0 atm, large numbers of particles could be obtained 3 h after the generating explosion. A shuttered sampler was built onto the floor of the chamber to capture settling particles at various times during the growth period, but it was rarely used.

The OPC, a Particle Measurement Systems LAS-X model, served mainly to monitor the particle concentration. The counts on the OPC channels served as a good indicator of the concentration on the filters. Pieces of the filters were mounted on stubs for observation in a scanning electron microscope (SEM), and the photographs taken on the SEM became the primary particle measurement technique.

The experimental results in the first year were a series of particle pictures taken at pressures of 1.0, 0.1, and 0.01 atm. Attempts were made to produce particles at 0.001 atm without success, and the question of the failure to produce particles has been deferred until the present year. The particle pictures that were taken show strikingly irregular structures, the kinds of structures that defy easy description. These early results changed the course of the investigation because it became clear that, although the structures were difficult to describe, there were definite pressure-related differences.

Liquid effects are important during the first few milliseconds of growth, and for longer times at lower pressures, but such effects are not relevant for most of the aerosol growth we have observed. Instead, we have concentrated on learning how to explain the unusual aspects of solid aerosol growth and applying those lessons to the changes we observed with pressure.

2.2 YEAR TWO

The work in year two was devoted mainly to developing an understanding of fractals and devising computer routines to assist in the analysis of the aerosol micrographs.

2.2.1 Theoretical Work

Fractals are self-similar geometrical figures that are scale invariant; they have the same appearance no matter what the scale of viewing is. It is clear that applying fractal analysis to real aerosol particles involves making certain distinctions in the fractal terminology. Exact fractals are geometrical structures that can be generated by an algorithm, and natural fractals are structures generated by some random process that follows a general rule. Exact fractals can conceptually be extended to all scales of observation, but natural fractals are bounded above by the finite size of the structure and below by the fundamental units making up the object. Thus, the natural fractal structures of the aerosols have a lower size limit imposed by the primary spherical particles that have formed the aerosol structure.

The natural fractals are also stochastic; i.e., they have random statistical variations. In a set of aerosols, it is to be expected that individual members will have somewhat different fractal dimensions, even after being generated by the same process. The average of the individual fractal dimensions can be expected to describe the characteristic of the aerosol structures.

The fractal dimensions associated with fractal objects is a measure of the structure of the objects. The fractal techniques we have used are one-dimensional descriptions of two- and three-dimensional objects. The fractal dimensions obtained for these one-dimensional descriptors are greater than 1 and less than 2.

One major interest in using fractals to characterize these aerosols is that considerable modeling work has been done on the fractal dimensions that result from different growth processes. These models have been computer simulations of structures growing by the accretion of small particles onto the larger ones or by the aggregation of clusters of similar size with one another, under the influence of Brownian (random walk) trajectories or straight line trajectories.

The models clearly separate particle-cluster and cluster-cluster growth according to fractal dimension. In particular, using the mass fractal definition, particles that collide with already existing clusters by Brownian diffusion exhibit a fractal dimension of 1.67 (5/3 theoretically). In higher dimensions, this is extended to:

$$D \tilde{=} 5/6d \quad , \tag{2-1}$$

where

d = spatial dimension from 2 to 6 [3,4].

The Brownian collision of clusters with clusters generally leads to a fractal dimension of 1.45 (for d = 2) or 1.75 (for d = 3) under a wide variety of assumptions, but there does not seem to be an exact value. These characteristic fractal dimensions also are generated by ballistic (straight line) trajectories, mainly because clusters cannot interpenetrate one another to any great extent.

If particle-cluster collisions occur ballistically (straight line trajectories), the fractal dimension is about 1.95, with a theoretical limit of 2 for infinitely small particles. The difference between 1.95 and 2 occurs because of the voids between tightly packed particles.

When dealing with images of particles (strictly two-dimensional), the question arises of how to relate the results to real three-dimensional particles. One answer is that for sparse particles, in which there is relatively little screening of parts of the image by other parts, the fractal dimension should be the same in two or in three dimensions [5]. Another answer is that the fractal dimension of the particle must obey a relation derived from causality [6]:

$$D_0 \geq d + 1 - D_1 \quad , \tag{2-2}$$

where

D_0 = particle fractal dimension

D_1 = fractal dimension of the trajectory of an incoming particle.

If the trajectory is Brownian, then D_1 is equal to the space dimension. If it is ballistic, the D_1 is 1. Therefore, the particle fractal dimension must fall between the rather broad limits of 1 and 2 for two-dimensional processes or between 1 and 3 for three-dimensional processes.

2.2.2 Experimental Work

In our use of fractals, we started with a tiling method, described in Reference [1], but had difficulty interpreting the results of an analysis of exact fractals. A tile could be counted as occupied either if a large fraction of it contained image pixels, or a very small fraction. The resulting fractal dimensions showed large variations, depending on the occupancy rule. Tiling is a process of approximating the area of an image, and other methods approximate the linear dimensions of the image. Tiling may prove useful in future investigations of aerosol particles in which area coverage is important, but it was abandoned in this one.

The remaining development of the analysis methods concentrated on three broad categories: perimeter measurements, dilation measurements, and correlation measurements. These have been recognized techniques for computing fractals, but there has been little standardization of the methods for analyzing images.

2.2.2.1 Perimeter Method--

In this method, the perimeter of an object is estimated by counting the number of steps of a given size required to circumscribe the object, and plotting it against the step size on a log-log plot. The fractal dimension of the perimeter is $1+|m|$, where m is the slope of the plot, assuming that there is a sufficiently long linear region to say that the object is indeed fractal in nature. An equation for expressing the perimeter as a function of the step size is:

$$P(r) \sim r^{1-D} \quad , \tag{2-3}$$

where

D = fractal dimension, between 1 and 2 in two dimensions.

The perimeter (or external hull) fractal does not take into account an object with interior perimeters, such as we see frequently in our micrographs. Furthermore, the perimeter fractal is not easily suited to computer analysis. On the other hand, the perimeter fractal does seem to be useful in picking out changes of shape between the primary spheres making up an object and the general shape of the object itself. At small scales, the perimeter approaches the geometric perimeter of the circles making up the particle image, and the

fractal dimension is close to 1. At larger scales, the perimeter bridges gaps around the particle, and the structure changes more rapidly with scale, giving a larger fractal dimension. We have observed some particles that were much longer along one axis than the other, and these particles show a return to a fractal dimension of 1 at scales between the length of the minor axis and the length of the major axis. Thus, in that range the particle behaves as if it were a one-dimensional structure.

2.2.2.2 Dilation Method--

A commonly used alternative definition of the fractal dimension is based on the distribution of mass around the center of mass of the object. If the object is fractal, the mass is given by:

$$M(r) \sim r^D \quad , \tag{2-4}$$

where

D = fractal dimension (less than the spatial dimension).

We have called this a mass fractal, but more accepted usage is the term "density fractal." The method used to calculate it is the dilation method because a series of boxes is expanded around the center of mass to determine the mass within each box.

In this case, r represents a "radius" of gyration around the center of mass. This fractal dimension definition is quite intuitive in its application because it corresponds closely with the fraction of area obscured by a particle. A sparsely distributed particle tends to have a low fractal dimension, closer to 1 than 2, and a densely distributed particle has a high fractal dimension, approaching 2.

It has been accepted practice to use square boxes in the method, but we think that, for comparison with other analysis methods, the expansions should be with circles. The difference between using boxes and circles is that the box method confuses the scale r by a factor of 1.4, blending some parts of the image that are farther from the center than others.

The expansion around the center of mass means that all the small-scale information is obtained from the region near the center of mass. This neglects small-scale information in other parts of the particle, unless auxiliary expansions are performed over all the particle.

At large scales, approaching the boundaries of the particle, the dilation method approaches a constant mass, the total mass of the particle, and the fractal dimension no longer has meaning. This boundary-limited behavior occurs at smaller scales when expansions are performed around centers other than the center of mass. Boundary effects on the mass fractal must be anticipated in the analysis, and the boundary-limited regions must not be given a fractal interpretation.

2.2.2.3 Correlation Method--

The correlation function is a relation describing the relative frequency of finding two parts of the image at a given distance from one another. It is an alternative way of calculating the density fractal. For fractal objects, the correlation function is related to the fractal dimension by:

$$C(r) \sim r^{D-d} \quad , \tag{2-5}$$

where

D = fractal dimension

d = spatial dimension.

Because the fractal dimension is less than the spatial dimension, the correlation function decreases with r.

Programs were written to calculate the correlation function directly and involved scanning the image, multiplying pixel values, and summing at various values for r. The process is manageable for small images and small values of r, but the time consumed in the calculation grows quickly for larger images. The correlation method does give a very complete picture of the fractal characteristics of the particles at small scales and seems to agree well with the dilation method at intermediate scales.

Both the mass and correlation fractals show similar behavior for a given particle and range of scales. The correlation function itself decreases with r, but if it is multiplied by r^2, then the result is very similar to the mass fractal:

$$r^2 \cdot C(r) \sim r^{D-d} r^d = r^d \quad , \tag{2-6}$$

because d = 2 for the images. In this way, it is feasible to use the dilation method to obtain the fractal characteristics at large scales, where it is a fairly efficient technique, and the correlation method at small scales, where it is effective.

3.0 SUMMARY OF PUBLISHED WORK FROM THE CURRENT YEAR

The fractal analysis methods as described have been adequate for the initial investigation. The dilation analysis has been expanded to include the circle dilation concept, where circles are the expansion element, rather than boxes. Several particles of various shapes have been compared with analyses by circle dilation, box dilation, and correlation. The results are being prepared for publication, as noted on the list of publications [6] in Section 7.0.

In general, the overall agreement between the box and circle dilations is good. However, as the dilations approach the size of the particles, the two methods give different results. Generally, when there is a change in the slope of the log-log curve, the change shows up more distinctly and at a smaller scale in the circle dilation method than in the box method. We attribute this to the more clearly defined scale lengths of the circle dilation.

The circle dilation and the correlation methods also generally agree over most of their common scale range, and the changes of slope occur at approximately the same scale lengths. For some particles, the correlation and dilation methods give indistinguishable results, but for others grown under the same conditions, the agreement is obviously poorer.

The sensitivity of the fractal analysis methods to changes in the shapes of the particles was the subject of substantial investigation. This consisted of a three-part program: analysis of multiple particles grown under identical conditions; analysis of simulated three-dimensional particles under different projections; and analysis of simulated three-dimensional mass distributions.

The density (mass) fractals of two groups of particles were measured on single micrographs taken at pressures of 1.0 and 0.1 atm. The micrographs were at a relatively low magnification, but the images were enlarged optically

with only a slight degradation of the resolution that could be attained with high magnification micrographs. The methods used were the correlation and circle dilation. The following table (Table 1) summarizes the results.

All of the resulting fractal dimensions are equal within the standard deviations of the averages. These numbers are consistent with the cluster-cluster growth in two-dimensions mentioned earlier. The visual appearance of these particles is also suggestive of clusters or chains of particles coming together. There are a few particles in each group whose fractal dimensions are quite low or quite high for cluster-cluster aggregation. The appearance of these deviant particles is not particularly unusual in comparison with the rest. The results of this analysis confirm the use of the density fractal as a consistent measure of the particle shape.

The second test involved the creation of an artificial particle. This could have been done with a physical model, but instead was done with a computer algorithm. The algorithm computed the centers of primary particles in three-dimensional space in a way that mostly retained the center of mass near the axes' origin, but it gave a reasonably random character to the particle. The particle could be viewed under different orientations and analyses in those projections. Under many orientations, the artificial particle resembled natural particles whose fractal dimensions had been previously determined. In those cases, the density fractal had a very similar dimension to the natural particles.

The size of the primary spheres making up the artificial particle could be varied at will. Values were chosen to (1) ensure that adjacent positions in the particle overlapped substantially; (2) cause occasional gaps between the primary spheres; or (3) to cause the primary spheres to be mostly isolated from one another. These cases are shown in Figure 2, where the primary sphere size varies across the columns and the orientation varies down the columns. The numbers at the bottoms of the columns show the mean and standard deviation of the dimensions in each column determined by the circle dilation and correlation methods.

Again, the two methods are in generally good agreement with one another. However, there is a strong variation of the fractal dimensions as the size of the primary particles decreases. This variation is indicative of the nature of the fractal analysis, namely that the object should be scale invariant over

TABLE 1. FRACTAL DIMENSIONS FOR PARTICLE ENSEMBLES

Pressure (atm)	Number of particles	D_c	D_d
1.0	15	1.40 ± 0.15	1.36 ± 0.15
0.1	10	1.35 ± 0.06	1.37 ± 0.09

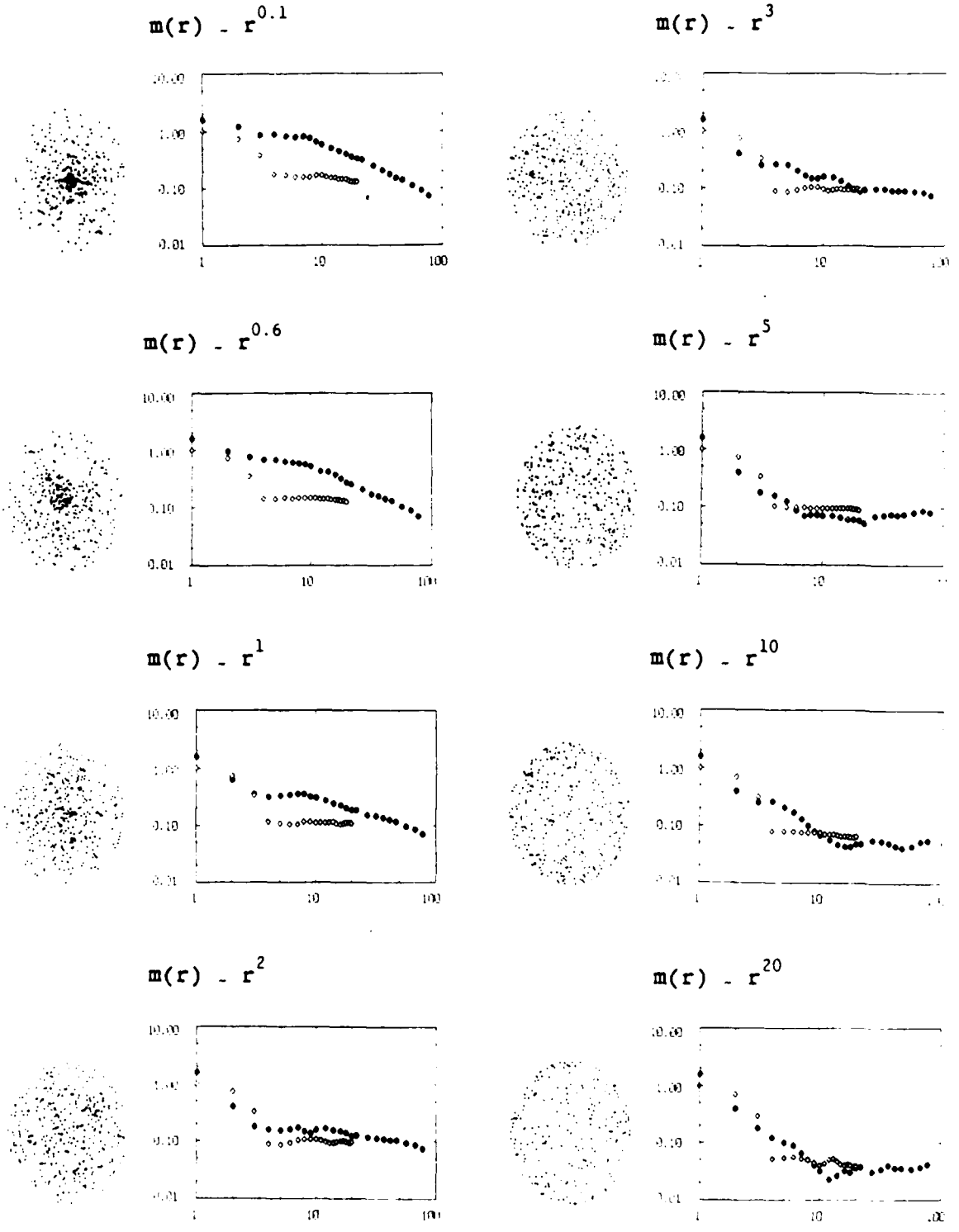

Figure 2. An artificial particle shown with different orientations and primary particle sizes.

a range of scales. The artificial introduction of gaps between the particles breaks the scale invariance at a scale comparable to the gap length. This can even be detected in some of the plots of the correlation and dilation functions.

The orientation effects with this artificial particle are within the range of variation of the natural particles and may be assumed to be negligible. The question of orientation will be addressed with natural particles in Section 4.0.

The last test of the sensitivity of the fractal analysis involved another set of algorithm-generated mass distributions, but this time with no attempt to construct contiguous spherical masses. Instead, mass distributions were generated in three dimensions by distributing point masses in a uniformly random fashion over the surfaces of concentric shells. The number of point masses in each shell was determined by a power-law relation between the total mass and the shell radius. The power-law exponents varied between 0.1 and 20 for the distributions. The point of the test was to see the ability of the fractal analysis to recover the three-dimensional mass distribution from the two-dimensional projected image.

The test cases and correlation/dilation plots are shown in Figure 3 for eight different power-law relations. This test should be counted a failure because neither the correlation nor the dilation could reproduce the generating power-law exponent. The correlation function was almost invariant for all the power laws used, and no information could be obtained from it. The dilation function, on the other hand, shows behavior that can be used to distinguish between different power laws. The fractal dimension computed from the slope of the curve does not, however, relate even semiquantitatively to the generating exponents.

These results show the main difference between the dilation and correlation methods. The correlation method examines all points in the space around a given point, while the dilation method examines all points at a fixed distance from the dilation center. The correlation method will pick up the influence of the gaps between mass points much more effectively than can the dilation method, whereas the dilation method will discern the overall mass distribution with radius. When the mass points occupy contiguous space, the two methods give very similar results.

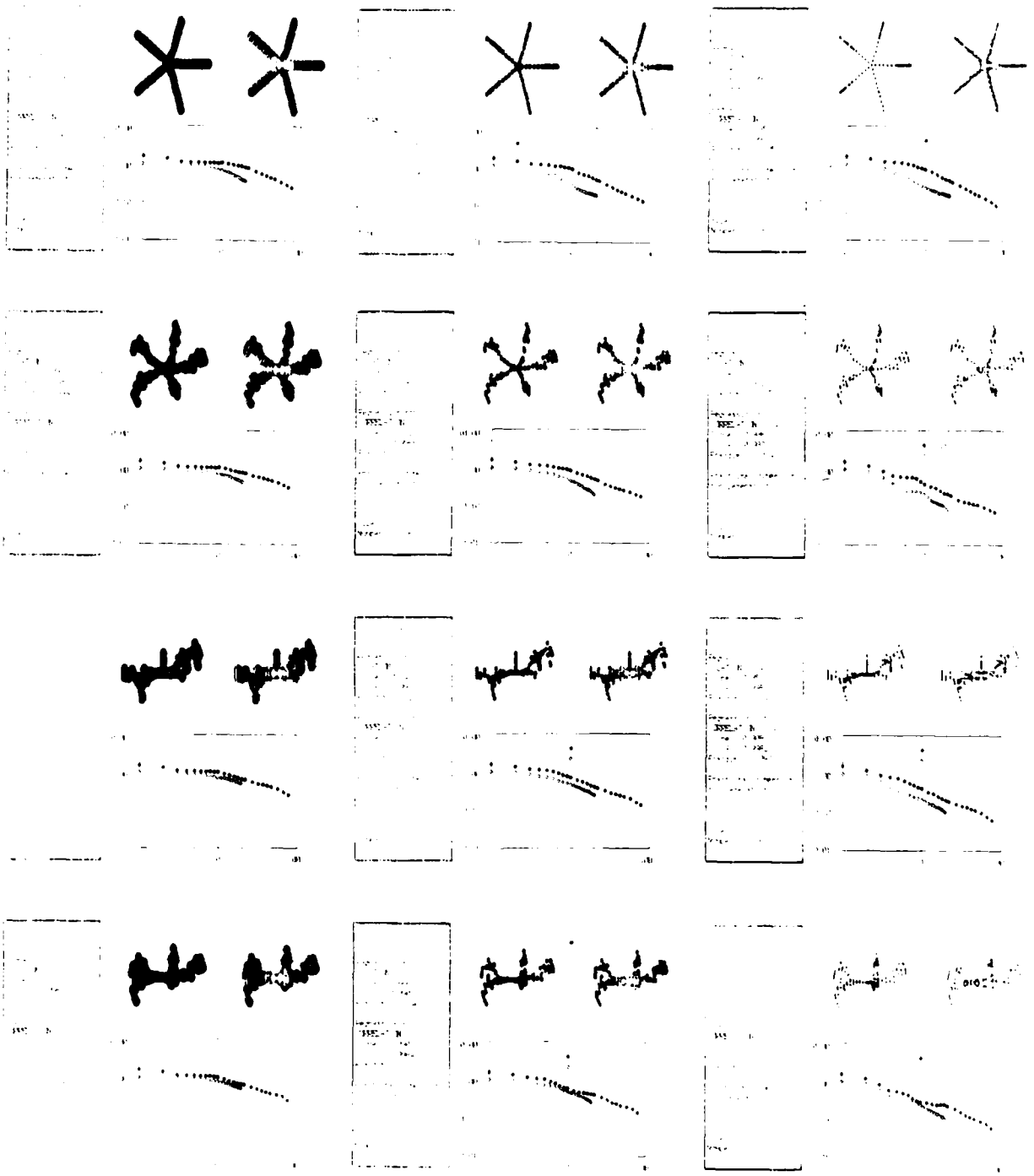

$F_1 = 1.37 \pm 0.07$
$F_2 = 1.35 \pm 0.17$

$F_1 = 1.22 \pm 0.13$
$F_2 = 1.05 \pm 0.14$

$F_1 = 1.18 \pm 0.09$
$F_2 = 1.09 \pm 0.06$

Figure 3. Distributions of mass according to a radial power-law and the correlation/dilation results for each distribution.

In light of Mandelbrot's statement about the fractal dimensionality of a projection of a fractal [5], it is not surprising to find that power-law exponents greater than 2 give strange results in the projection. The dilation plots for generating exponents less than 2 do give extended ranges of power-law behavior, consistent with fractal character. However, the fractal dimension does not reflect the generating power-law exponent.

Further reflections on the character of three-dimensional fractals led us to conclude that all projections of such objects will have dimensions of about 2 when the three-dimensional structure has a dimension greater than 2.

4.0 DETAILS OF UNPUBLISHED WORK OF THE CURRENT YEAR

The remainder of the final year's effort has been devoted to answering some of the questions that have occurred in the course of the work. Broadly speaking, these are the questions of the universality of the phenomena we have observed, the problems of generating particles at low pressures, the effects of electric fields on the growth of the aerosol, the effects of covaporization of other materials with the metal, the nature of the fractal analysis under actual rotation of the specimens, and the primary particle size distribution under various gas pressures.

We will consider these questions and the answers produced in the experiments in the following sections.

4.1 CONFIRMATORY RESULTS WITH OTHER METALS

Our approach for confirming the universality of the results we obtained with silver aerosol was to use a variety of other metals under the same conditions. This meant using metals with higher and lower melting boiling points, which would simultaneously allow us to explore electrical charging of the aerosols during the explosion phase and the low pressure formation problems.

Time limitations prevented a total survey of the metals that were available. Table 2 shows the ones tested and the associated physical properties that are important.

This selection covers a wide range of melting and boiling points. A previous report [7] had pointed out our difficulties in generating aerosols with aluminum. These attempts had been made in air atmospheres, and no particles were observed, either visually or with an OPC. When the aluminum wastried once more in a nitrogen atmosphere, the aerosol formed was comparable visually to that formed from other metals, strongly suggesting that the previous failures were due to the oxidation of the molten or vaporized aluminum.

TABLE 2. METALS USED FOR AEROSOL GENERATION

Element	Melting point (°C)	Boiling point (°C)	Density (g/cm^3)
Silver	961	1,950	10.5
Indium	156	1,450	7.3
Tin	232	2,260	7.3
Zinc	419	907	7.1
Molybdenum	2,620	4,507	10.2
Platinum	1,773	4,300	21.5
Iron*	1,535	3,000	7.9
Aluminum*	660	2,057	2.7

*Aerosols from these metals were not collected, but simply observed visually.

With the exception of the zinc, the metals all formed spherical primary particles. The zinc formed crystallites somewhat larger in mean size than the others. The subsequent coagulation of all the materials was similar. Micrographs of the various metals under different conditions are shown in Appendix B.

The density fractal dimensions of these materials are summarized in Table 3.

4.2 ANALYSIS OF LOW-PRESSURE PROBLEMS

After repeatedly failing to generate and observe any particles at all with silver at 0.001 atm, we raised the pressure until particles were observed at 0.002 atm. Other metals exhibited similar behavior, with complete failure to generate particles below 0.002 atm. There are individual differences from metal to metal, but we have localized the critical pressure to within only a factor of 2.

Understanding the explosion process itself may help identify the cause for this behavior. The details of the explosion follow the general steps listed below [8]:

1. The flow of current heats the wire to its melting point. Inertia and magnetic fields contain the molten wire and allow current to continue flowing.

2. The wire is heated well above its vaporization point. It is superheated because the time scale is too short for equilibrium boiling. In a reduced gas pressure, it may not heat to the same temperature as in a high-pressure atmosphere.

3. Vapor pockets form in the liquid, but heating continues as long as there is a continuous path in the liquid.

4. Vaporization disrupts the current flow. The remaining liquid filaments coalesce into spherical droplets.

5. Thermionic emission causes the droplets to emit electrons and become positively charged. Because the vapor density is high, electron multiplication is suppressed.

6. The vapor expands rapidly. The liquid droplets are carried into regions of decreasing vapor concentration. In the decreasing vapor, electron multiplication takes place, and the arc may re-strike.

TABLE 3. DENSITY FRACTALS FOR METALLIC AEROSOLS

Element	Pressure (atm)	D_c	D_d
Silver	1.0	1.40 ± 0.15	1.36 ± 0.15
	0.1	1.35 ± 0.06	1.37 ± 0.09
	0.01	1.70 ± 0.02	1.60 ± 0.02
	0.002 -- Minimum for formation		
Indium	1.0	1.38 ± 0.08	1.41 ± 0.13
	0.01	1.47 ± 0.20	1.42 ± 0.24
	0.005	1.54 ± 0.12	1.54 ± 0.11
	0.002	1.49 ± 0.11	1.47 ± 0.10
	0.005 -- Minimum for significant formation		
Tin	1.0	1.58 ± 0.12	1.47 ± 0.12
	0.01	1.51 ± 0.06	1.49 ± 0.08
	0.002 -- Minimum for formation, only single particles		
Zinc	1.0	1.38	1.45
	0.01	1.59	1.51
	0.004 -- Minimum for formation		
Molybdenum	1.0	1.56	1.53
	0.01*	1.68	1.74
	0.002	1.29	1.33
	0.002 -- Minimum for formation		
Platinum	1.0	1.40	1.55
	0.01*	1.56	1.64
	0.002	1.30	1.40
	0.002 -- Minimum for formation		

*See the section on low-pressure problems (Section 4.2) for additional information.

This analysis of the wire breakup has been supported by high-speed X-ray photographs of wires. The mechanisms leading to breakup may not be unique, but it is clear that some liquid droplets remain from the original wire. It is not totally vaporized by the electrical current.

Now, the superheated liquid droplets expand into the sample chamber where competing processes take place. First, there is cooling by the ambient gas. There is potential continued evaporation of the material from the droplets, and there is potential condensation of metallic vapor onto the droplets or spontaneous nucleation and growth of new droplets.

The minimum radius that can support continuous growth is given by the Kelvin equation:

$$r_c = 2Ms/RTd\ln S \quad , \tag{4-1}$$

where

r_c = particle radius

M = molecular weight of metal

s = surface tension of metal (850 dyne/cm)

R = gas constant

T = temperature of metal

d = density of metal

S = saturation ratio [9].

If the radius is less than this critical value, the droplet will ultimately evaporate. If the radius is larger, it will grow. The problem in applying this relation is the great uncertainty about the experimental situation.

Under the steps leading to the formation given above, the temperature of the liquid drop must be at least equal to the normal boiling point of silver, 2,483 K. If the superheating is substantial, the temperature might be as high as 2,600 K. It is also not clear that the ambient pressure could affect this temperature strongly. The saturation ratio is definitely an equilibrium concept: the ratio of ambient partial pressure to the vapor pressure at the surface of the particle.

Calculations of the critical radius over a range of temperatures corresponding to boiling at 0.001 atm up to 7 atm (1,560 to 5,040 K) produce a very narrow range of critical sizes. For S = 1.01, the critical radius decreases from 0.18 to 0.05 μm. For S = 1.02, the range is 0.09 to 0.03 μm, and for S = 1.05, the range is 0.04 to 0.01 μm. These results are right in the range of primary particles encountered. Any particles formed with smaller radii than these will evaporate. Any larger ones will grow. Table 4 summarizes the critical radius (diameter) calculations for a number of materials and includes mean primary particle diameters measured on micrographs of the particles.

The calculated critical diameters and measured primary particle sizes are in reasonably good agreement for saturation ratios of 1.05 and are generally in poor agreement for saturation ratios of 1.01. The critical diameters for the various metals are reasonably close to one another at a given saturation ratio. This agreement is strengthened in the experimental measurements of particle diameters, where relatively minor differences exist. The outstanding exception is for zinc at 1.0 atm. The measured diameter is considerably higher than for the other metals, or for zinc at lower pressures. In the micrographs, the primary particles of zinc appear to be small crystals rather than solidified spheres. This crystallization suggests that the formation process is significantly different and probably involves the slow cooling of droplets that had not completely vaporized.

The uncertain variables in this calculation are the surface tension, which is rarely available over the temperature range of interest, and the equilibrium vapor pressure. The use of a constant saturation ratio implicitly assumes that the ambient pressure sets the vapor pressure of the vaporized metal within the ratio factor. Thus, at 0.01 atm, we have assumed the vapor pressure of the metal is 7.6 Torr and that the temperature of the vapor is equal to the equilibrium temperature at that pressure. The measurements of primary particle diameter are also susceptible to sampling and statistical error because the micrographs are at their limit of resolution and, at most, contain a few hundred primary particles.

Nonetheless, the calculations show that the primary particles tend to be larger as the pressure is lowered, and the saturation ratio of 1.05 is of the

TABLE 4. CRITICAL DIAMETERS FOR METALLIC AEROSOL FORMATION

Element	Pressure (atm)	Surface tension (dyne/cm)	Diameter S=1.01 (μm)	Diameter S=1.05 (μm)	Diameter measured* (μm)
Silver	1.0	850	0.17	0.03	0.060
"	0.1	850	0.20	0.04	0.045
"	0.01	850	0.24	0.05	0.061
Indium	1.0	515	0.23	0.05	0.053
"	0.01	515	0.25	0.05	0.064
"	0.004	515	0.26	0.05	0.050
"	0.002	515	0.26	0.05	0.067
Tin	1.0	480	0.17	0.03	0.069
"	0.01	480	0.22	0.04	0.042
"	0.002	480	0.24	0.05	0.038
Zinc	1.0	763	0.29	0.06	0.126
"	0.01	763	0.40	0.08	0.049
"	0.004	763	0.043	0.09	0.041
Molybdenum	1.0	2,080	0.20	0.04	0.064
"	0.01	2,080	0.25	0.05	0.054
"	0.002	2,080	0.28	0.06	0.047
Platinum	1.0	1,700	0.16	0.03	0.040
"	0.01	1,700	0.22	0.05	0.049
"	0.002	1,700	0.25	0.05	0.047
Aluminum	1.0	860	0.04	0.01	--
Iron	1.0	1,800	0.21	0.04	--
Copper	1.0	1,200	0.14	0.03	--
Magnesium	1.0	502	0.25	0.05	--

*Count median diameter (CMD).

right magnitude. From these results, theoretical estimates of primary particle size can be made, as has been done in Table 4 for aluminum, iron, copper, and magnesium.

This prediction of the primary particle sizes still does not answer the low-pressure formation problem. Examination of the chamber walls after each explosion at 0.001 atm showed the presence of spots of the metal that could only have been deposited in the molten state. Different metals showed different diameter spots. At the slightly higher pressures for which aerosol formation occurred, there was still evidence of the spots, but it was not as plentiful.

The conclusion that we reach from these consistent observations is that the exploded metal droplets collide with the walls of the chamber before evaporating. The flight path is approximately 55 cm from the wire to the wall where the spots were observed. Raising the gas pressure to 0.002 atm stops most of the droplets for most metals within this distance, allowing them to evaporate. Although the stopping distance does depend on gas and particle density, particle radius, and initial velocity, it is worthwhile to examine the relations that can be derived.

The stop distance for high-velocity particles is well above the Stokes' law range and is given by:

$$s = \frac{4}{3}\,\rho_p'\rho_g d \quad dRe\ C_D Re \quad , \tag{4-2}$$

where

s = distance

ρ_p = particle density

ρ_g = gas density

d = particle diameter

Re = particle Reynolds number, which depends on velocity

C_D = drag coefficient, which also depends on Reynolds number [9].

The Reynolds number for particles is given by:

$$Re = \frac{vd\rho_g}{\mu} \quad , \tag{4-3}$$

where

v = particle velocity

d = particle diameter

μ = gas viscosity.

The drag coefficient, C_D, is a dimensionless quantity that depends on the Reynolds number. For the intermediate turbulent range, $2 < Re < 800$, the drag coefficient varies as $Re^{-1/2}$, and for the turbulent range, $Re > 1{,}000$, it is constant for all practical purposes.

Assuming that the droplets are all generated with the same dimaeters and initial velocities, the stopping distance will mainly depend on the inverse of the gas density. Therefore, the stop distance will vary inversely with pressure.

From this result, a change of pressure by a factor of 2 can make the difference between droplets stopping entirely within the chamber or being deposited on the chamber walls. If we assume a stop distance of 50 cm at 0.002 atm, then we can extrapolate to higher and lower pressures. The results are shown in Table 5.

We see from the table that laboratory production of aerosol by an exploding wire generator will become impractical below 0.001 atm because the size of the chamber required to stop the droplets in the gas is excessive. The rate of coagulation and growth of the primary particles is also a function of their concentration, once formed. As the gas pressure is reduced, even assuming that the stopping distance is within the confines of the chamber, the average concentration decreases with the third power of the stopping distance.

One final problem that had been anticipated originally appeared at low pressures. For the molybdenum and platinum wires, the explosion failed to destroy the wire. In fact, only a very small fraction of the mass was evaporated, and the wires showed no signs of melting. Aerosol particles were produced, although at much lower concentrations than expected.

The explanation for the persistence of the wires is that the surge of current through the wires caused rapid heating, but the resistance of the wires also increased with temperature. This allowed the voltage across the wire to increase to the point that gas breakdown occurred, shunting the remaining energy from the capacitor into the gas. The breakdown strength of the gas is proportional to gas pressure, and this breakdown would be expected to occur first at the lowest pressures. The high melting points of the platinum and molybdenum allow the temperatures and resistances to increase substantially without losing the integrity of the wire.

TABLE 5. STOP DISTANCE AS A FUNCTION OF PRESSURE

Pressure (atm)	Stop distance (cm)
10.0	0.01
1.0	0.1
0.1	1
0.01	10
0.001	100
0.0001	1,000
10^{-5}	10^{4}
10^{-6}	10^{5}

4.3 MAJOR ELECTRIC FIELD EFFECTS

Metallic aerosols are particularly susceptible to electric field effects because even electrically neutral particles can experience strong dipole polarization and torques in an electric field. The concentration of an electric field at the extremities of a conducting particle causes strong gradient forces there, which leads us to expect that the random agglomeration patterns will become much more linear. This has been borne out in computer models of agglomeration with long-range forces [10].

Initial observations of different materials in the EWG using a Plexiglas chamber showed that some materials, particularly iron, formed extensive chains, while others, such as silver or copper, did not [1]. The suspected low charge on the silver aerosol was confirmed with Faraday cage measurements.

The visual observation of chain formation is considered a good indicator of electric fields influencing aerosol growth. However, in the metal chamber, the observed chain growth was confined to the metal posts supporting the wire before the explosion and the bolt heads nearby. The probable reason for this phenomenon is as follows.

Any cloud of charged aerosol particles is self-dispersive. That is, the charges on the particles causes them to repel one another and the cloud expands. The equation governing the motion is quite general and easy to calculate if the particle mobilities are known. In the Plexiglas chamber, the charged particles are quickly deposited on the chamber walls, but they do not lose their charge. From those positions on the walls, their charges create electric fields in the chamber that continue to influence the growth of the remaining neutral particles and agglomerates. In the metal chamber, on the other hand, the particles caught on the walls lose their charges instantly and can no longer influence the agglomeration.

The electrodes and the bolts near them can have residual potentials on them, due to the circuitry, and so are in a position to collect particles on dendritic chains, if enough charge exists initially. The presence of dendritic growths, and their degree, is also considered a measure of the charge on the aerosol particles from the explosion. Table 6 summarizes the observations of dendrite growth.

The observation of charge effects is roughly in proportion to the melting points and not to the boiling points. Even with the variation of materials,

TABLE 6. METALLIC DENDRITE OBSERVATIONS

	Melting point (°C)	Boiling point (°C)	Dendrite formation
Silver	961	1,950	Very slight
Indium	156	1,450	None
Tin	232	2,260	None
Zinc	419	907	Very slight
Molybdenum	2,620	4,507	Moderate
Platinum	1,773	4,300	Moderate
Iron	1,535	3,000	Considerable
Aluminum	660	2,057	None

Note: Approximately five times the normal amount of material was exploded for the iron wire, leading to the heavier dendrite formation.

none of the centimeter-long chains, which were so obvious in the Plexiglas chamber, was observed in the metal chamber. The longest particle that was observed was roughly 1 mm in length (for molybdenum). Therefore, an additional electric field source was placed in the chamber through a Plexiglas plate for observation.

The source was a 1.8 in. diameter rod connected to a high voltage power supply. When this rod is centered in the 12-in. diameter chamber, the electric field at any radial distance from the center is given by:

$$E(r) = V/[r \ln(r_c/r_r)] \quad , \tag{4-4}$$

where

r_c = chamber radius

r_r = rod radius.

Voltages of 200 to 20,000 V were applied to the rod after a molybdenum wire explosion. The application of any voltage within this range led to dramatic formation of chains of up to a centimeter in length, but additional effects were observed.

The chains either carried an initial charge or formed in contact with either the chamber wall or the rod because there was a steady, rapid drift of chains toward or away from the rod. At the higher applied voltages, the chains would accelerate in one direction or another, but they would be arrested in flight as a piece of the chain broke off and carried the attracting charge to the electrode. The remainder of the chain, carrying a repulsing charge, was driven in the opposite direction. This motion of the chains had the effect of scavenging the chamber of small particles very quickly, and the concentration dropped many times faster than it would have done without the action of the electric field.

In this case, the electric field was strong enough for the differential forces on the ends of the chains to cause the breakage of them. The constant electric field also caused any particles in contact with the wall or rod to acquire an induced charge. For many particles, the force on the induced charge was strong enough to lift them from the surface into flight, but the majority remained on the walls permanently.

These observations strongly support the role of electric fields in the formation of the chains. The stronger the field, the faster the chains grow,

both because of the attraction of neutral particles to the end of the chain and because of the motion of the chain through the relatively stationary neutral cloud.

Although time was not available for us to collect aerosol particles grown under these conditions, the agglomerated aerosols from the higher-melting-point materials do show evidence of more chainlike growth than the low-melting-point materials do.

4.4 COVAPORIZATION CONFINEMENT

Covaporization of a metal and another material was a part of the projected work in this last year's effort. The reason for doing this is that many aerosol-generating schemes always involve more than one component, either deliberately or through contamination. The shock from the exploding wire would have enough energy to vaporize or shatter a foil wrapped around the wire, and it would produce a mixed aerosol environment in which the growth of the metallic aerosol could be substantially modified.

An experimental explosion was performed with a silver wire inserted into a small piece of Teflon tubing before being mounted in the generator. Although the Teflon was chosen mainly for convenience, a dielectric such as Teflon would have a likelihood of acquiring charges during disruption and affecting the subsequent growth of the aerosol.

The explosion of the wire did vaporize much of the tubing, but several pieces were recovered from the chamber floor after the explosion. Low-power microscopic examination of the larger pieces showed that molten droplets were embedded in them, much like the molten droplets that had impacted the chamber walls. Small particles of material, presumably Teflon, were observed to be attracted to the electrodes after the explosion, but the number did not increase after the first few minutes.

In all other respects, the growth of the silver aerosol followed the usual course, with the particles growing in size until they could be distinguished visually, and then decreasing slowly by settling. There was no macroscopic evidence of altered growth. Time prevented the pursuit of microscopic samples.

4.5 FRACTAL STABILITY UNDER ROTATION

The problem of using fractal analysis methods on three-dimensional particles in two-dimensional micrographs was approached in two ways. The first

is reported in Reference [7], where an artificial particle was computer-generated in a way that allowed it to be rotated and projected from any point of view. Several views of this particle are shown in Figure 3.

Although the apparent fractal dimension changes with the size of the primary particles, viewing across the rows, the fractal dimensions under rotation, viewing down the columns, are in reasonable agreement. The standard deviation of the different orientations is comparable to the standard deviation for particle ensembles in Table 1.

The second approach was to view some naturally formed particles at different orientations (indium at 1.0 atm). This was done by tilting the SEM stage at various angles before taking micrographs. (This technique is often used to make stereoscopic pairs for the detection of three-dimensional features.) A group of indium particles was found that offered a variety of particle shapes; pictures were taken with the electron beam at angles of 0, 30, 50, and 74 degrees with respect to the normal. The fractal dimensions for five of these particles are presented in Table 7. Two of the particles are shown in Figure 4, where it can be seen that the character of the particles does not change strongly for most orientations. The scales of these figures are not all the same, as they would be if taken directly from the micrographs. These are edited images taken from the computer screen.

The results of this test are a good indicator of the error in the density fractal dimension that could be expected from orientation effects. It is of the same order as the expected variation from particle to particle. The standard deviations compare favorably with those for the theoretical particle orientation.

We conclude that the analysis of two-dimensional images can be used successfully to obtain the three-dimensional fractal dimensions of aerosol particles, at least as long as the fractal dimension is strictly less than 2.

4.6 PRIMARY PARTICLE SIZE DISTRIBUTIONS

Visual inspection of the micrographs gives the impression that the primary particle size becomes smaller and more varied as the pressure is lowered. During the digitization of the primary particles, the size distributions were computed. A simple measure of the width of the distribution is given by the ratio of the mass median diameter (MMD) to the count median diameter (CMD). The MMD is computed as the diameter that divides the total particulate mass

TABLE 7. ORIENTATION EFFECTS FOR NATURAL PARTICLES

Particle #		0	30	50	74	Avg
1	F_c:	1.39	1.44	1.43	1.41	1.42 ± 0.03
	F_d:	1.33	1.40	1.40	1.41	1.38 ± 0.05
2	F_c:	1.30	1.26	1.32	1.31	1.30 ± 0.03
	F_d:	1.33	1.55	1.49	--	1.46 ± 0.14
3	F_c:	1.46	1.49	1.48	1.58	1.50 ± 0.06
	F_d:	1.49	1.55	1.55	1.49	1.52 ± 0.04
4	F_c:	1.31	1.18	1.29	1.45	1.31 ± 0.13
	F_d:	1.40	1.20	1.41	1.71	1.43 ± 0.24
5	F_c:	--	1.79	1.76	1.79	1.78 ± 0.02
	F_d:	--	1.85	1.81	1.96	1.87 ± 0.10
					R.M.S. deviation	0.11

R.M.S. = Root mean square.

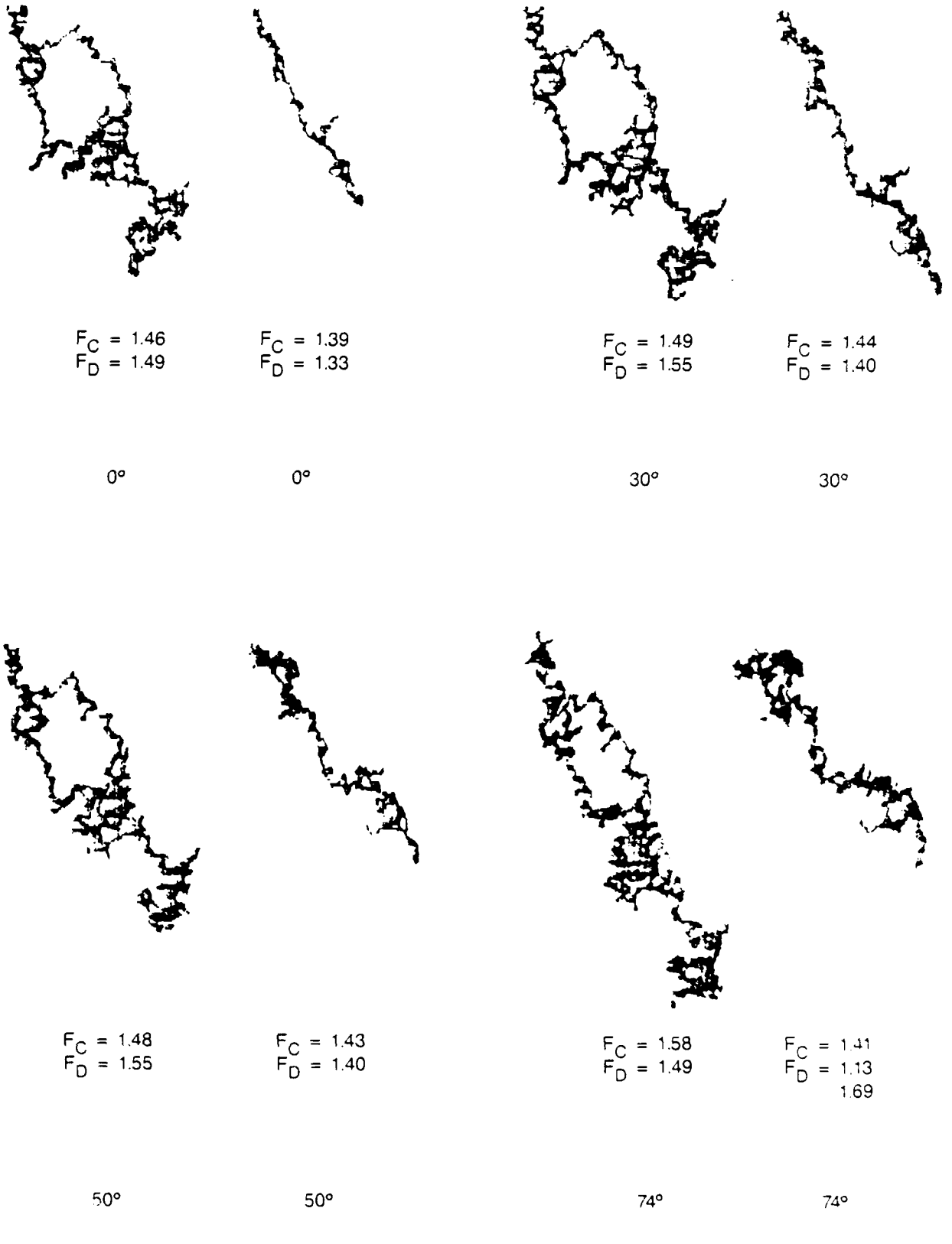

Figure 4. Two particles viewed with different orientations of the SEM stage.

into two equal halves, and the CMD is the diameter that divides the particles into two groups of equal numbers.

If the primary particles are all the same size, then the MMD and the CMD are equal. As the distribution includes more particle sizes, the MMD grows faster than does the CMD because of the volume dependence of mass. Therefore, the more polydisperse the distribution is, the greater the ratio between MMD and CMD. Table 8 summarizes the results for all the metals measured.

From the table, it can be seen that the silver and indium results are responsible for the impressions cited above. Both have a much more nearly monodisperse primary distribution at 1.0 atm than the others, and the ratio increases at the lower pressures. The other metals give a much less clear indication.

It is tempting to speculate that the initial size distribution is nearly monodisperse at all pressures and that the increasing polydispersity at lower pressures is the result of liquid (molten) particle coagulations in the first few seconds of growth before solidification. The coagulation process should lead to more polydisperse primary particles, ultimately growing into the distributions shown in Figure 1. Although we think this interpretation is qualitatively correct, there is not enough evidence to conclude so quantitatively.

4.7 DISCUSSION

Before coming to conclusions about the results presented, we would like to summarize the computer model results published for two- and three-dimensional aggregation (Tables 9 and 10, respectively).

Now that we are confident that the two-dimensional fractal analysis gives us the fractal dimensions in three dimensions, for $D < 2$, we must abandon interpretations of the aerosol behavior based on two-dimensional models. The two-dimensional models describe the aggregation of particles confined to a plane, such as on the surface of a liquid. Their use is inappropriate for aerosol formation with three-dimensional growth characteristics. This means that the range of fractals that we have encountered, with dimensions from about 1.2 to 1.8, must be measured against the results for the three-dimensional models.

Concentrating on the Table 10, we see that only the cluster-cluster aggregation results give fractals in the proper range to describe the fractals

TABLE 8. PRIMARY PARTICLE DISTRIBUTION RATIOS

Element	Pressure (atm)	CMD (μm)	MMD (μm)	Ratio	Particles
Silver	1.0	0.06	0.076	1.27	1,013
"	0.1	0.045	0.060	1.33	1,114
"	0.01	0.061	0.089	1.46	654
Indium	1.0	0.053	0.068	1.28	267
"	0.01	0.064	0.099	1.55	318
"	0.005	0.050	0.070	1.40	211
"	0.002	0.067	0.103	1.54	243
Tin	1.0	0.069	0.106	1.54	515
"	0.01	0.042	0.057	1.36	202
"	0.002	0.038	0.063	1.66	86
Zinc	1.0	0.126	0.182	1.44	118
"	0.01	0.049	0.082	1.67	284
"	0.004	0.041	0.058	1.42	29
Molybdenum	1.0	0.060	0.090	1.50	81
"	0.01	0.054	0.089	1.65	121
"	0.002	0.047	0.066	1.40	58
Platinum	1.0	0.040	0.066	1.65	400
"	0.01	0.049	0.071	1.45	288
"	0.002	0.047	0.076	1.62	1,106

CMD = Count median diameter.

MMD = Mass median diameter.

TABLE 9. FRACTAL DIMENSIONS OBTAINED FROM TWO-DIMENSIONAL AGGREGATION MODELS

Model	D
Linear trajectory, particle-cluster	1.95 ± 0.002
Brownian trajectory, particle-cluster (theory)	1.6667
Brownian trajectory, particle-cluster	1.73 ± 0.06
Linear trajectory, cluster-cluster	1.50 ± 0.05
Brownian trajectory, cluster-cluster	1.44 ± 0.02

TABLE 10. FRACTAL DIMENSIONS OBTAINED FROM THREE-DIMENSIONAL AGGREGATION MODELS

Model	D
Linear trajectory, particle-cluster	2.97 ± 0.08
Brownian trajectory, particle-cluster (theory)	2.5000
Brownian trajectory, particle-cluster	2.45 ± 0.1
Linear trajectory, cluster-cluster	1.81 ± 0.03
Brownian trajectory, cluster-cluster	1.75 ± 0.05

we have encountered. The nature of cluster-cluster aggregation obscures the differences between the trajectories because clusters tend to penetrate each other very little, whether or not they travel in straight lines.

Our computer analysis results for distributions of particles show that very few differences can be distinguished for power-law mass distributions with exponents of 2 or greater. This is consistent with the lemma that fractals of dimensionality <2 can be measured in two dimensions. During the course of the experiments, we have encountered clumps of particles that probably result from gravitational scavenging of small particles by large clusters. These have a dense appearance and a density fractal dimension near 2 (1.93 by correlation, 1.84 by dilation.) Presuming that these clumps exhibit a three-dimensional fractal dimension of about 2.97 (for linear trajectory, particle-cluster interactions), the fractal dimension of their projection is indeed almost equal to 2.

This means that the fractal analysis of images cannot distinguish any three-dimensional characteristics with dimensionality greater than 2, i.e. particle-cluster aggregation. The conclusion we must then draw is that fractal dimensions of 1.6 to 1.8 in the micrographs represent cluster-cluster aggregation only. This is reasonable in light of the predominance of clusters in the micrographs, but it leaves unanswered the mechanism responsible for the measured fractals in the range 1.2 to 1.5 that are generally more prevalent than are the higher values.

The lower fractal dimensions indicate that some mechanisms are present that are not accounted for in the standard models. The apparent fractal dimension in the range of two-dimensional cluster-cluster aggregation causes us to consider the possibility of forces that confine the motions of the particles to two dimensions. These might be either electrical forces or shear forces.

Shear forces arise when a velocity gradient exists in the gas. The part of the particle in the higher velocity region attempts to move faster than the part in the lower velocity region. This results in an orientation force that tends to move the particles into the higher velocity region. Consider two particles moving in the gas near one another. If the velocity shear is essentially planar, as occurs for gas moving near a flat wall, and the particles are at different distances from the wall, they will travel with significantly

different velocities and spend little time near each other. Therefore, the chances of their diffusing to one another and sticking are small. If, however, they are at the same distance from the wall, they will spend a long time near each other, even though both are moving with respect to the wall, and have a much higher probability of colliding.

If the particles are moving at slightly different distances from the wall and slightly different velocities, then they may collide in a grazing configuration and stick together. This also has the effect of confining the relative motion to a plane because any cross-flow movements would reduce the probability of collision greatly.

Thus, motion in a shear flow can have the effect of confining the diffusive motion to a plane and might result in a large fraction of the particles having the two-dimensional cluster-cluster characteristic.

Electric fields have been shown to have a pronounced effect on the particles in causing the chain structures to grow. Electric fields also play a role in orienting complex particles. The presence of an electric field induces charge separation (polarization) in any metallic conductor. Positive and negative charges move apart until their separation causes a field that exactly cancels the external field in the interior of the conductor.

These separated charges can be acted on by the external field to create torques on the particle. The torques tend to orient the particle so that the longest axis of the particle points in the direction of the field. Any diffusive motion between particles will tend to take place along the field direction in preference to the other directions because the polarization charges on one particle tend to attract the polarization charges on another particle along the field lines. If the particles approach each other on parallel field lines, the polarization charges tend to repel each other. This is the reason for the formation of chains, but it also tends to bring the two particles into contact at their extremities.

Of the two forces, we think the electric field mechanism is more likely because the evidence of particle charges is already confirmed by the formation of dendrites and chains. Any shear motion would have to be driven by the turbulence immediately after the explosion or by convective motions near the walls after the gas in the chamber has become quiescent.

Still, the appearance of the low fractal dimension in the particles provides an indication of the growth processes that occurred during the lifetime of the particle.

4.8 CONCLUSIONS

The conclusions we can draw from this work are as follows:

1. Metallic aerosol can be formed from a molten or vapor state in the laboratory down to a pressure of about 0.001 atm. Formation at lower pressures becomes exceedingly difficult and may require much larger active volumes and initial mass of material.

2. Metallic aerosol particles can be produced in an inert gas atmosphere from the molten state. In the presence of oxygen, the aerosol will generally be an oxide (nonmetallic).

3. The melting point of the material controls the degree of charges associated with the disruptive process in the exploding wire generator. In another form of generator, such as a thermal source, the charging might not be as significant, but it would be expected to follow the same order for materials.

4. The primary particles formed are usually spherical and are consistent with a condensational growth. The average diameter of the particles is in good agreement with theory, using a saturation ratio of 1.05, approximately. There is surprisingly little variation of primary particle size from metal to metal, but exceptions may be found, namely, aluminum.

5. There is a slight trend toward forming smaller primary particles as the gas pressure is lowered. There is a definite trend toward forming more polydisperse primary particles as the gas pressure is lowered. This may arise from standard processes involving liquid droplet coagulation in which the primary particles remain molten for longer periods at reduced pressures.

6. Fractal analysis methods for micrographs of aerosol particles are now well-developed. Correlation and dilation techniques give results in good agreement with one another. The perimeter fractal analysis is less appropriate for aerosol growth studies.

7. Fractal analysis of particles does distinguish differences in growth mechanisms. Without the guidance of models, however, the information obtained would be difficult to relate to growth processes.

8. The fractal analysis of images gives reliable fractal dimensions for characteristic fractals less than 2 in three dimensions. It cannot distinguish fractal characteristics that would have dimensions greater than 2.

9. Fractal analysis is not sensitive to the orientation of the particles, within reason. The variation of fractal dimension with orientation is of the same order as from particle to particle within an ensemble of particles.

10. For the aerosols studied, three-dimensional cluster-cluster aggregation ($D \cong 1.7$) is the dominant growth mechanism.

11. There is substantial evidence of microscopic charge effects in the aerosol growth, represented by chain formation and low fractal dimensions ($D \cong 1.4$).

12. Gas pressure affects the density fractal dimension. It generally increases as the pressure is reduced. This means that the aerosol structures are more compact at lower pressures. The trend is toward ballistic aggregation at pressures below 0.001 atm, but this has not been verified experimentally.

5.0 IMPLICATIONS OF THIS WORK FOR SPACECRAFT SURVIVABILITY

In this section, we discuss some of the implications of this program on the overall spacecraft survivability issue.

The generation and growth of metallic aerosols in a vacuum environment would require one of two conditions: (1) a generation technique substantially different from the exploding-wire generator, or (2) an artificial, low-pressure atmosphere. The experiments have shown that a critical saturation ratio is needed to foster the growth of primary particles and that a finite time is required for the molten droplets produced in the EWG to evaporate and cool.

This time is available in the laboratory because the droplets are halted by the ambient gas. In the orbital vacuum, the cooling would be by radiation only, and it would take a significantly longer time. During that cooling time, the particle cloud would have expanded far beyond the dimensions we have used in the laboratory.

A different generator principle would allow the dispersion of primary particles into the vacuum, but their subsequent growth would still be determined along the lines of this investigation. Aggregation of primary particles in a vacuum would be by ballistic trajectories, without question. Therefore, the aggregates would be compact, almost solid bodies, unless some external forces cause some preferential collision directions.

Orbital mechanics would create a shearing velocity field: Those particles in lower orbits will move with a higher velocity, and those in higher orbits will move with a lower velocity. Grazing contacts between particles would give a tendency toward chains and clusters, but with a much lower rate than diffusive motion would.

The elongated, open structures of the aerosol particles we have produced would be effective electromagnetic radiation scatterering centers because their cross-section is roughly equivalent to a solid of the same diameter at the wavelengths of interest. These structures cannot form without some diffusive motion unless the clusters making them up are preformed. Even if clus-

ter subunits were dispersed into the vacuum, growth would be slow without diffusion or differential velocities to cause collisions.

After exposure in the vacuum environment for a period of time, the particles would begin to be charged by the ionized species present and by photoelectric emission from exposure to sunlight. The development of a net unipolar charge would hasten the dispersal of the particulate cloud, whereas the development of bipolar charges from the photoelectric effect would encourage chain formation. Other factors influencing the rate of dispersal of the cloud are its initial ejection velocity from the parent craft and the difference in orbital velocities between the parent and the cloud, and between parts of the cloud.

The maximum control of the growth and dispersal of a particulate cloud would occur in a confined environment with a suitable gas atmosphere. The concept of a large balloon is the most obvious method of maintaining this control. With a captive gas atmosphere, the boundaries of the initial dispersal can be set by the stopping distance of the initial particles. The subsequent coagulation and growth rates can be controlled by determining the concentration of particles and gas pressures. Containment of the cloud also minimizes problems of spurious contamination and of removing the cloud when desired.

6.0 REFERENCES

1. Study of Mean Free Path Effects on Growth of Ultrafine Metallic Aerosols. Year One Report (June 1985).

2. Study of Mean Free Path Effects on Growth of Ultrafine Metallic Aerosols. Year Two Progress Report (March 1986).

3. Meakin, P. Phys. Rev. A 27, 1:604-607 (1983).

4. Meakin, P. Phys. Rev. Lett. 27, 3:1495-1507 (1983).

5. Mandelbrot, B. B. The Fractal Geometry of Nature. W. H. Freeman, San Francisco (1982).

6. Ball, R. C., and Witten, T. A. Phys. Rev. A 29, 2966-2967 (1984).

7. Lawless, P. A. Particle Generation by Exploding Wires. Presented at the 1986 CRDEC Scientific Conference on Obscuration and Aerosol Research.

8. Lawless, P. A., P. C. Reist, and M.-T. Hsieh. Sensitivity of Fractal Analysis for Describing Particle Shapes. Presented at the 1987 CRDEC Scientific Conference on Obscuration and Aerosol Research.

9. Reist, P. C. Introduction to Aerosol Science. Macmillan, New York (1984).

10. Richter, R., L. M. Sander, and Z. Cheng. J. Colloid. Interf. Sci. 100, 203-209 (1984).

7.0 CUMULATIVE LIST OF PUBLICATIONS AND PRESENTATIONS

Fractal Characterization of the Structure of Aerosol Agglomerates Grown at Reduced Pressures. M-T. Hsieh, P.A. Lawless, and P.C. Reist. Submitted to Aerosol Science and Technology.

Generation and Growth of Metallic Aerosol at Subatmospheric Pressures. P. A. Lawless, P. C. Reist, and M.-T. Hsieh. Presented at Fine Particle Society Annual Meeting, Boston, 1987.

Sensitivity of Fractal Analysis for Describing Particle Shapes. P. A. Lawless, P. C. Reist, and M.-T. Hsieh. Presented at the 1987 CRDEC Scientific Conference on Obscuration and Aerosol Research.

Mean Free Path Effects on Particle Coagulation. P.A. Lawless, P.C. Reist, and M-T. Hsieh. Proceedings of the 1985 CRDC Scientific Conference on Obscuration and Aerosol Research. (R.H. Kohl, ed.).

Particle Generation by Exploding Wires. P.A. Lawless. Presented at the 1986 CRDEC Scientific Conference on Obscuration and Aerosol Research.

Preliminary Study of the Growth of Metallic Aerosols Under Reduced Pressure Environment. Master's Thesis. Ming-Ta Hsieh. University of North Carolina, Chapel Hill (1986).

PROFESSIONAL PERSONNEL

P. A. Lawless, Ph.D. Principal Investigator, Research Triangle Institute

P. C. Reist, Ph.D. Co-Investigator, University of North Carolina

APPENDIX A

MICROGRAPHS OF VARIOUS METALS UNDER DIFFERENT CONDITIONS

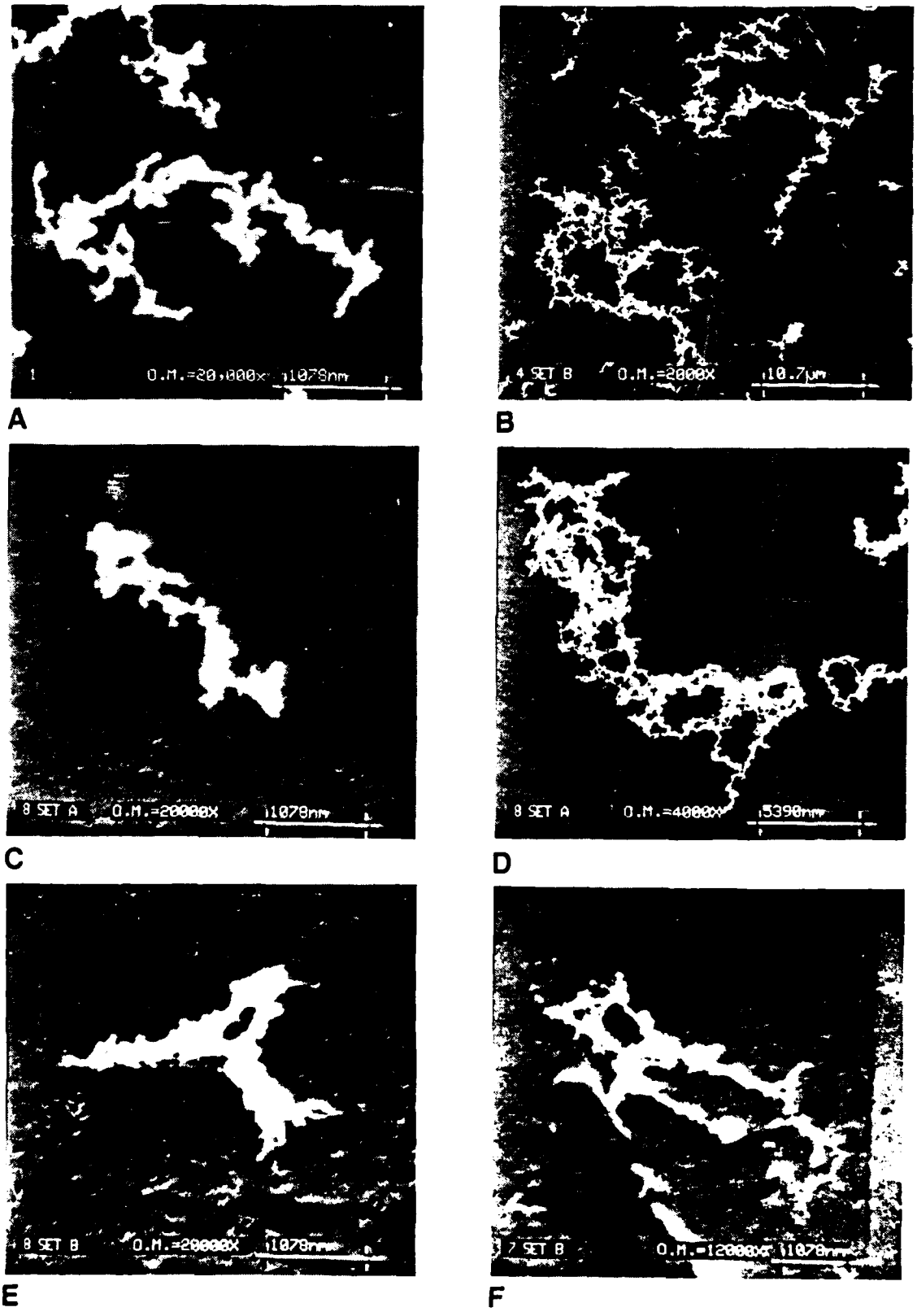

Figure A-1. Silver aerosol: A,B — 1.0 atm; C,D — 0.1 atm; E,F — 0.01 atm.

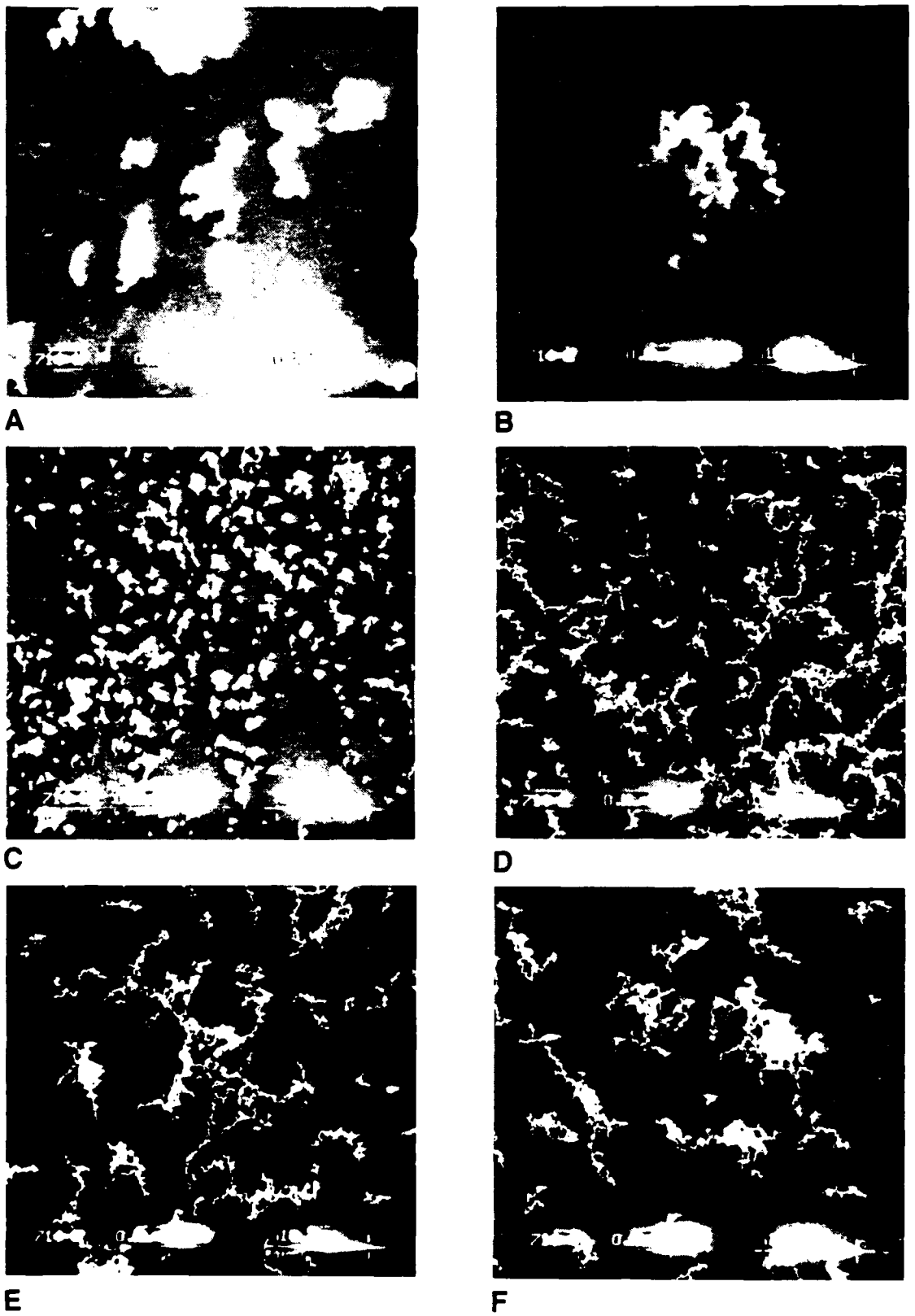

Figure A-2. Indium aerosol: A-F — 1.0 atm.

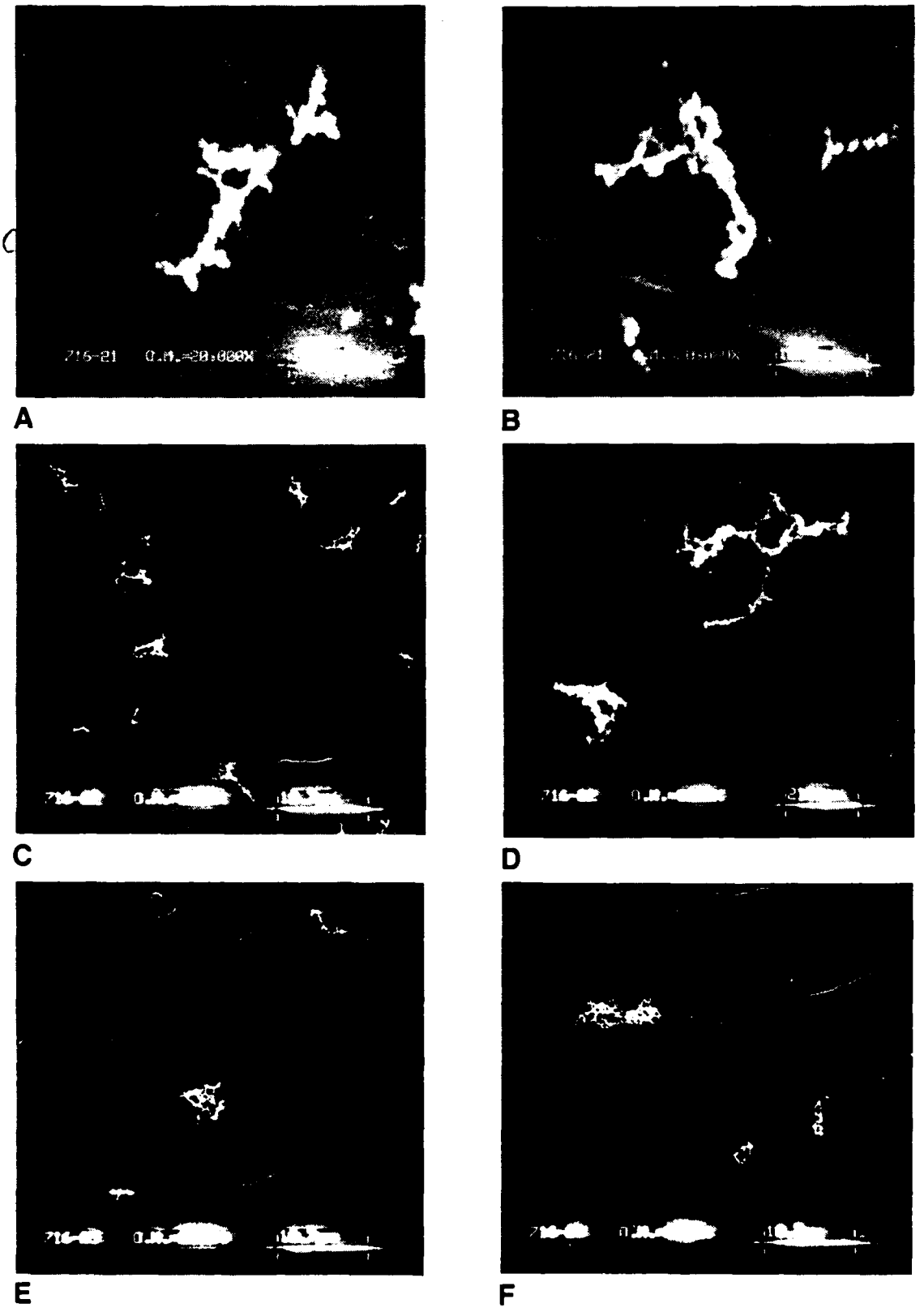

Figure A-3. Indium aerosol: A-F — 0.01 atm.

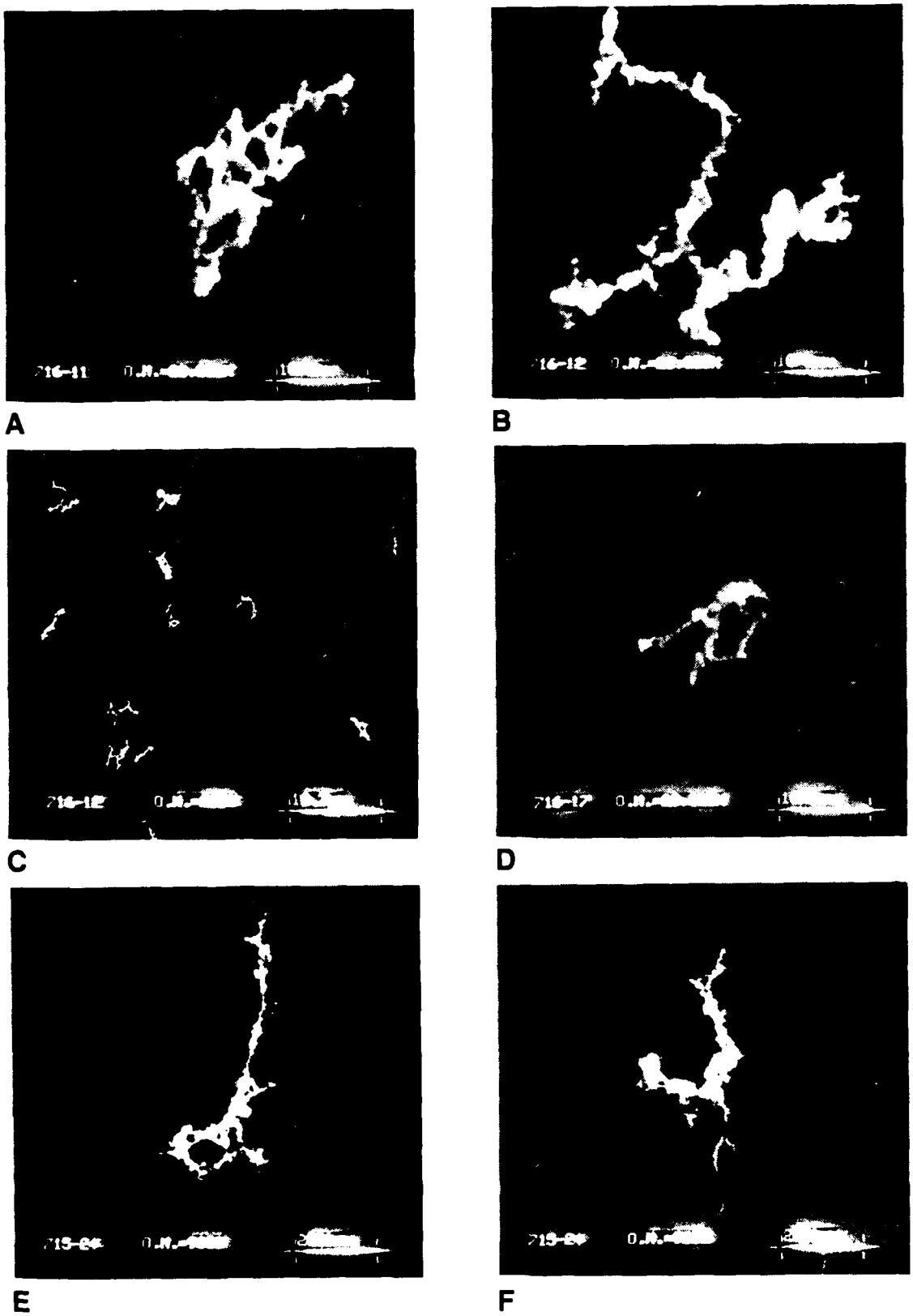

Figure A-4. Indium aerosol: A-D — 0.005 atm; E,F — 0.002 atm.

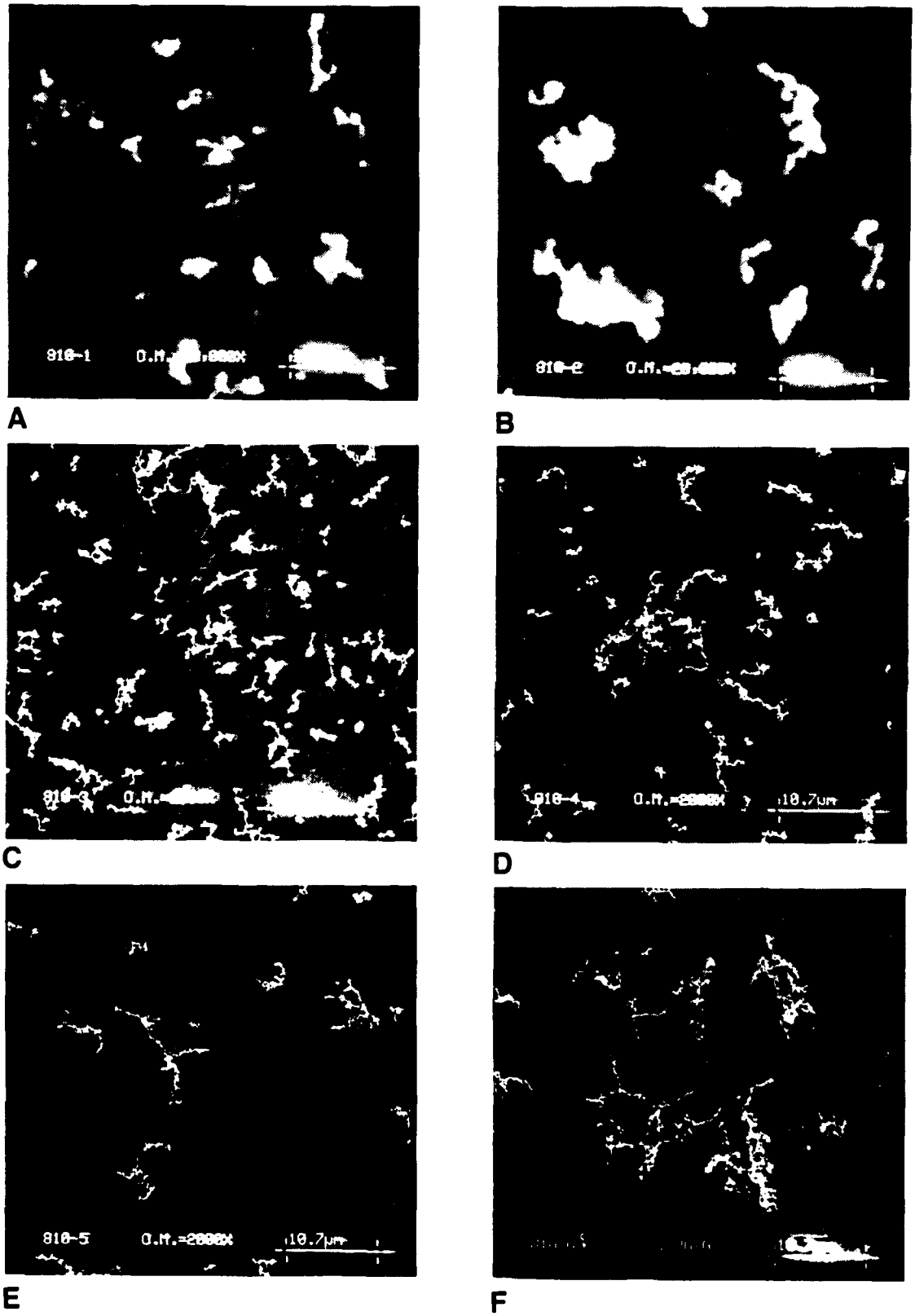

Figure A-5. Tin aerosol: A-F — 1.0 atm.

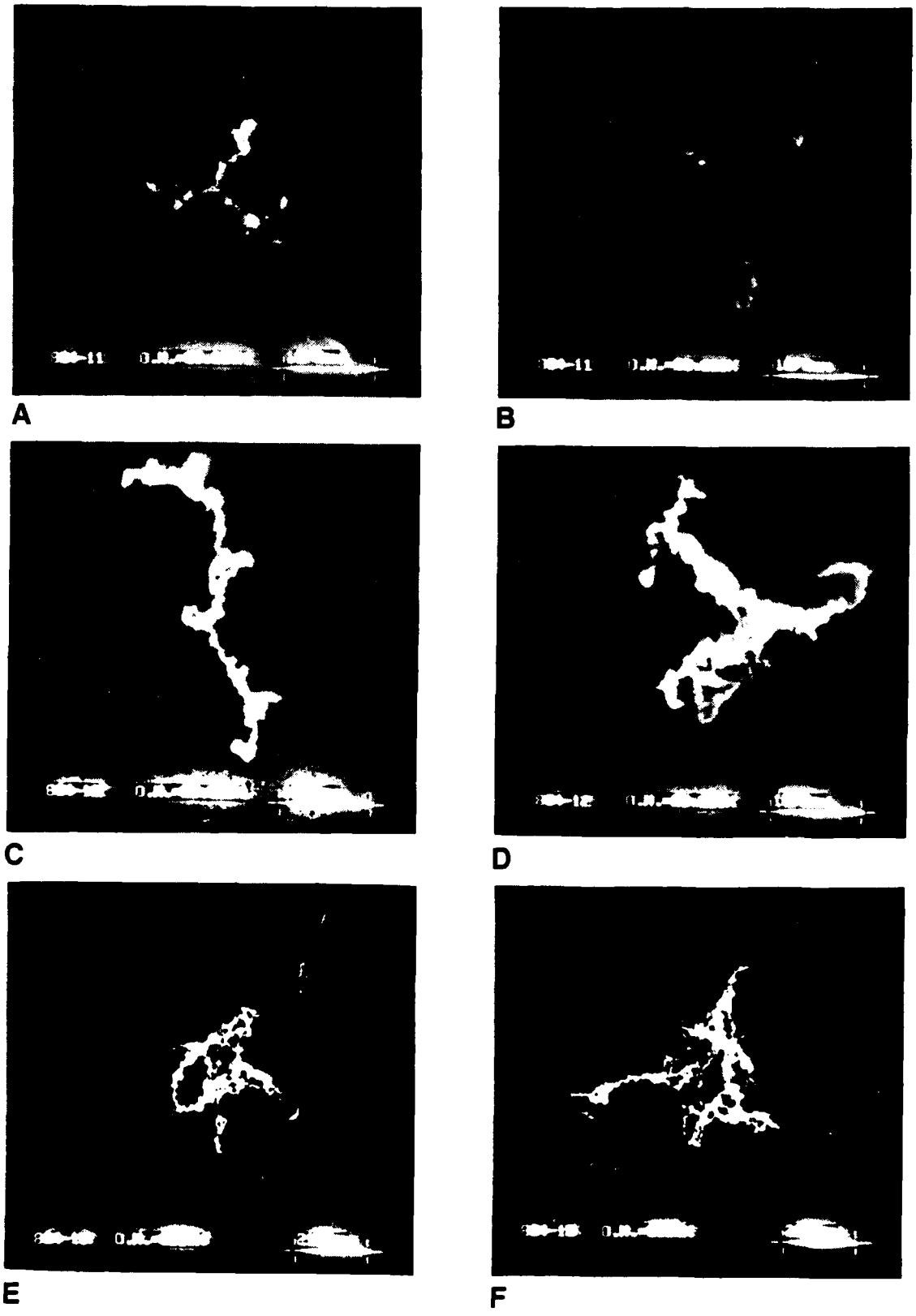

Figure A-6. Tin aerosol: A-F — 0.01 atm.

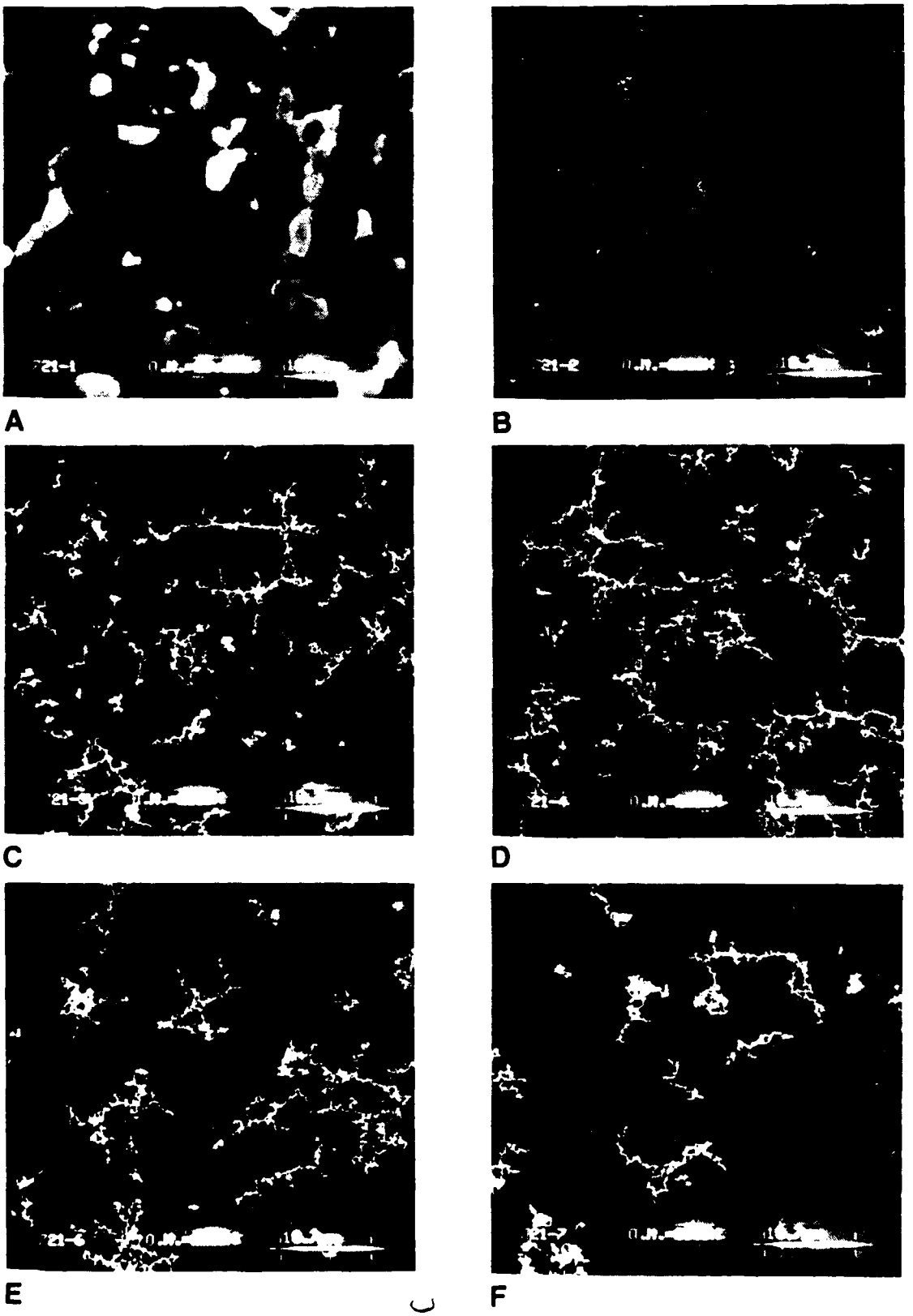

Figure A-7. Zinc aerosol: A-F — 1.0 atm.

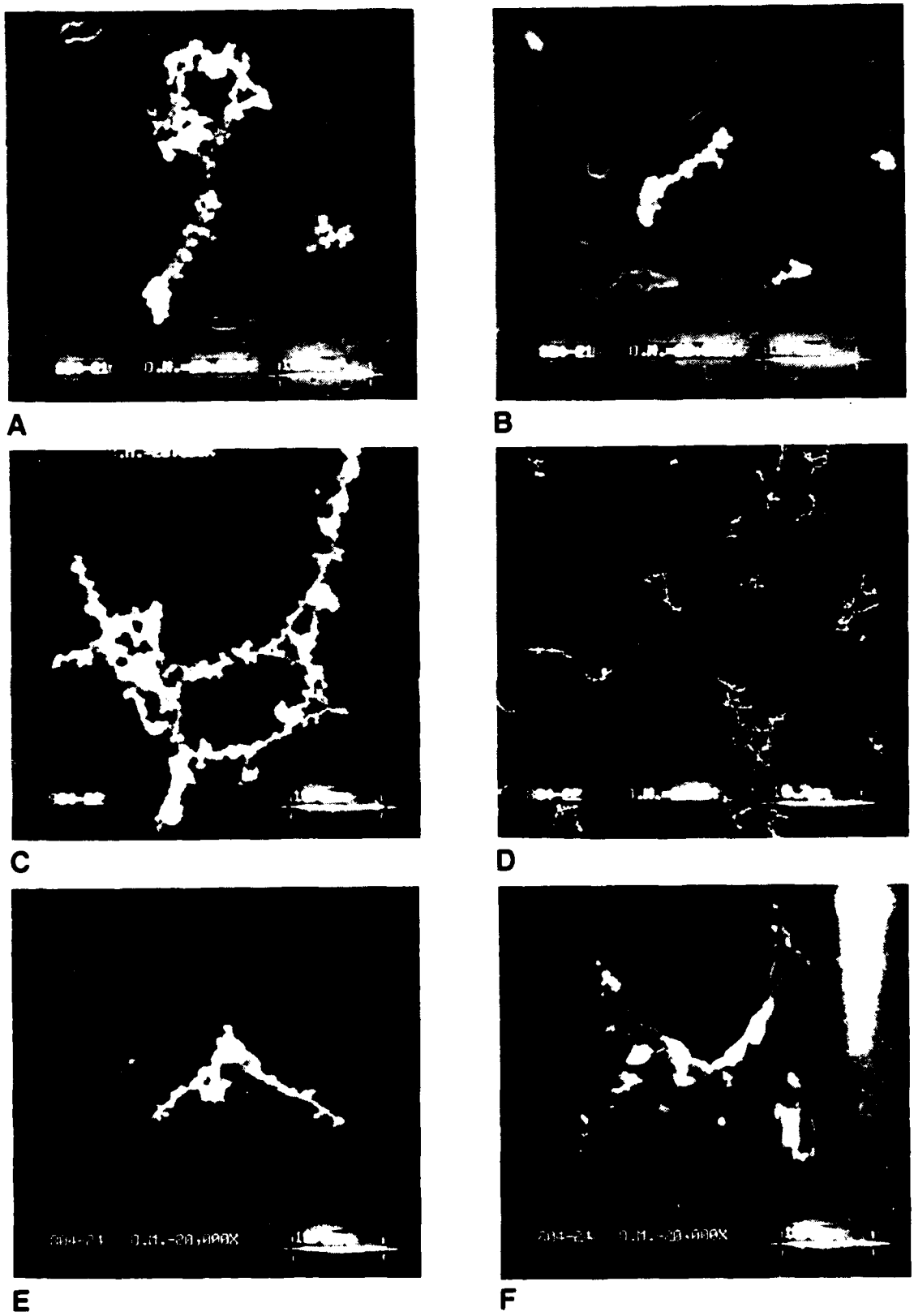

Figure A-8. Zinc aerosol: A-F — 0.01 atm.

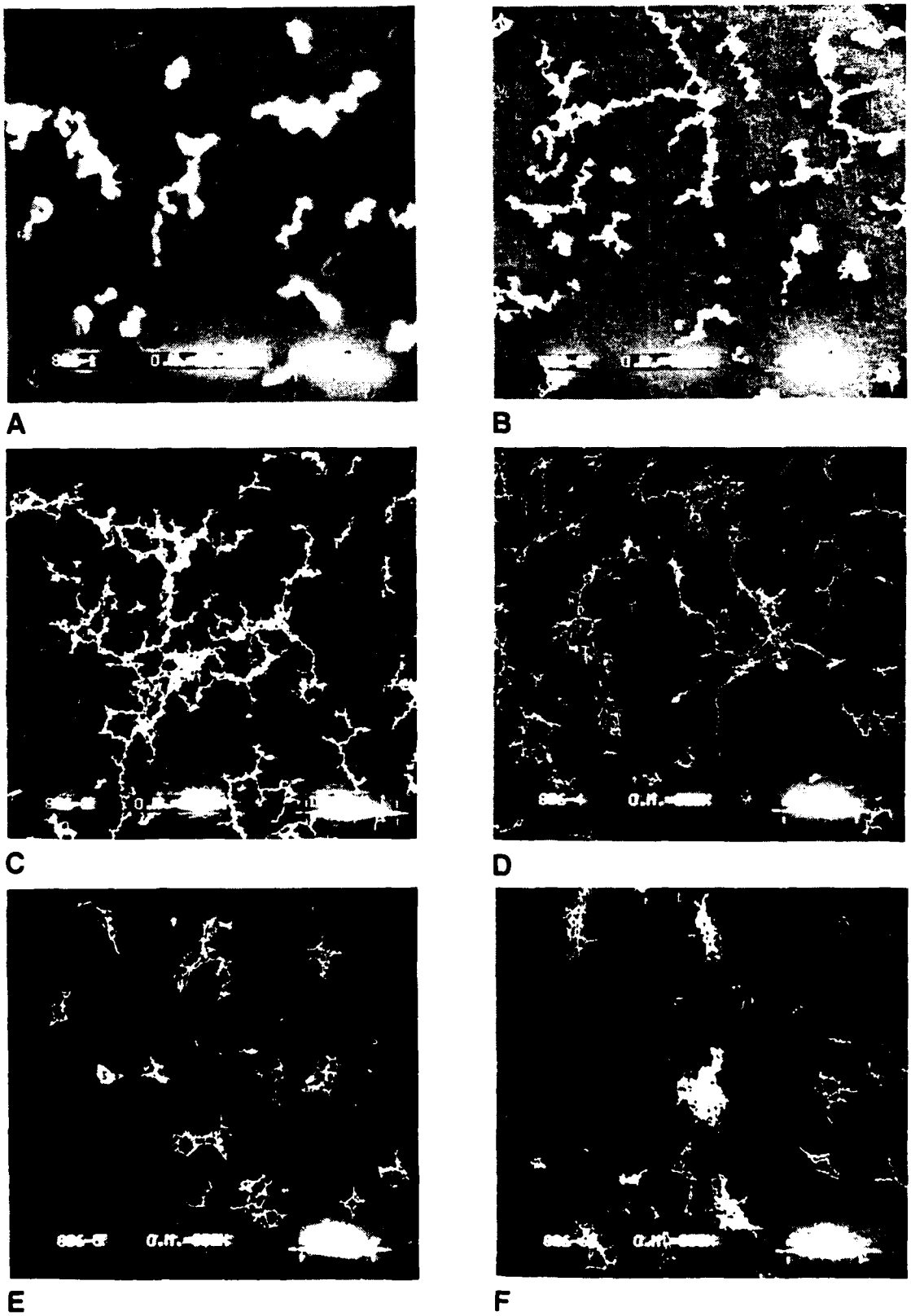

Figure A-9. Molybdenum aerosol: A-F — 1.0 atm.

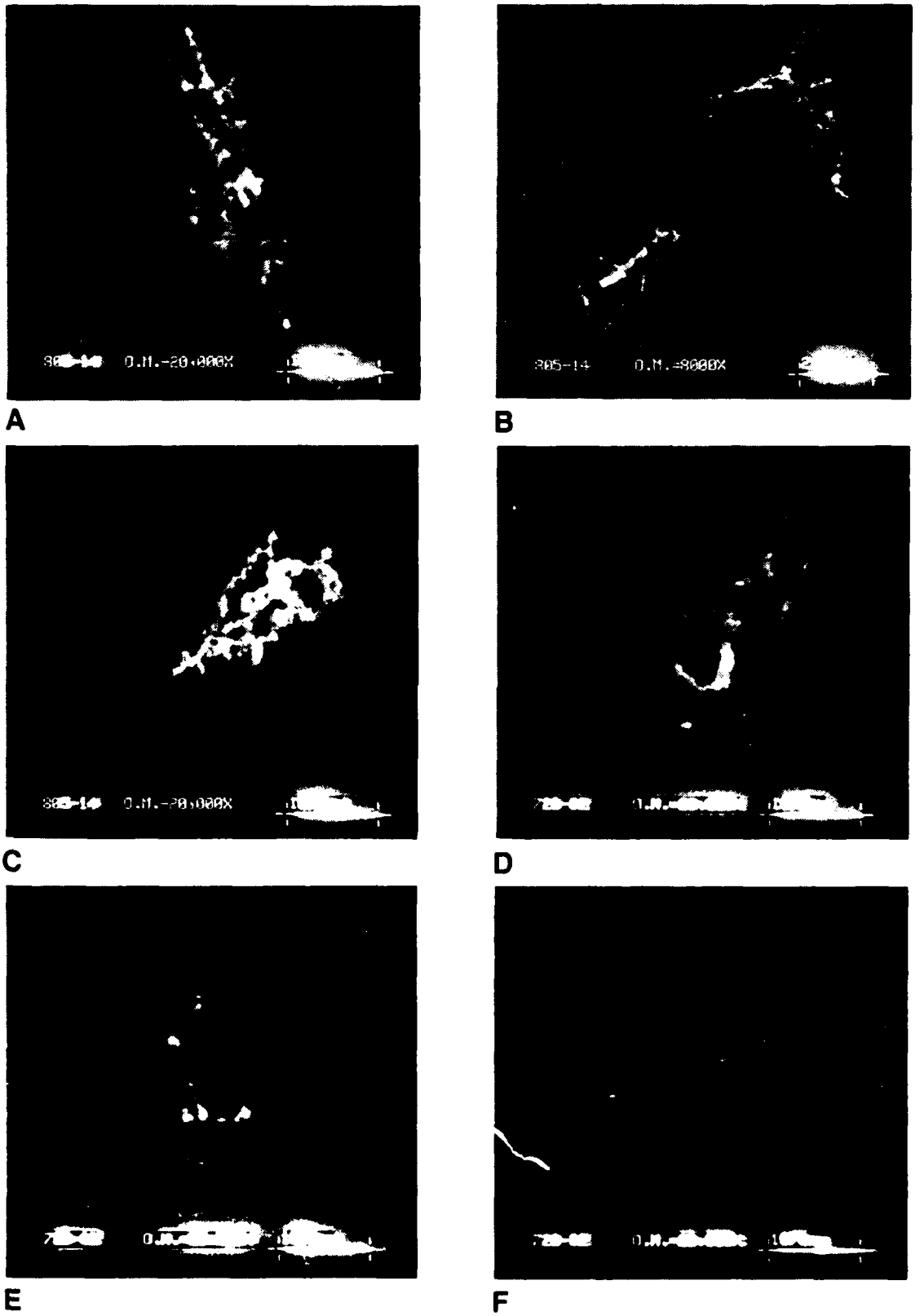

Figure A-10. Molybdenum aerosol: A-C — 0.01 atm.; D-F — 0.002 atm.

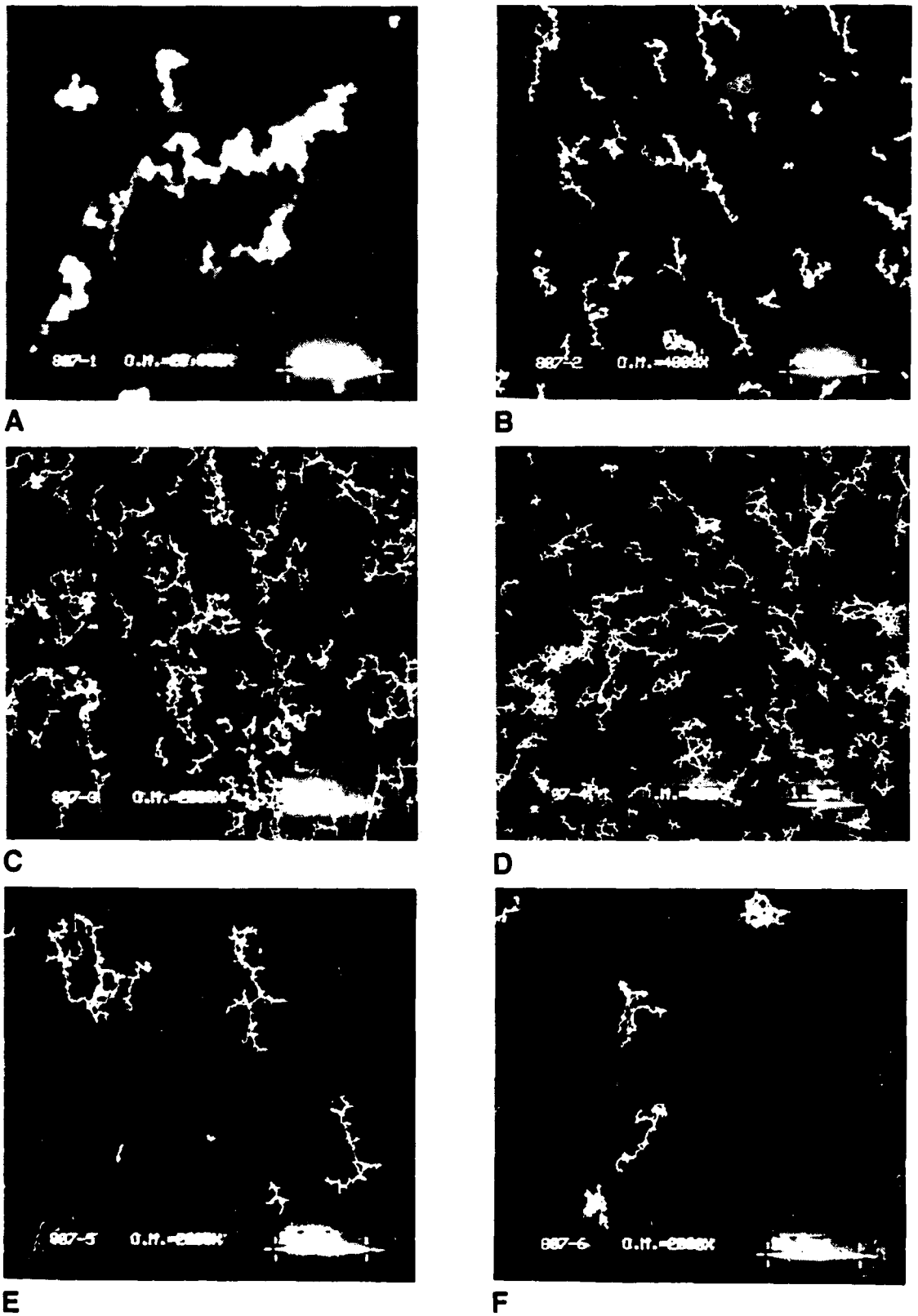

Figure A-11. Platinum aerosol: A-F — 1.0 atm.

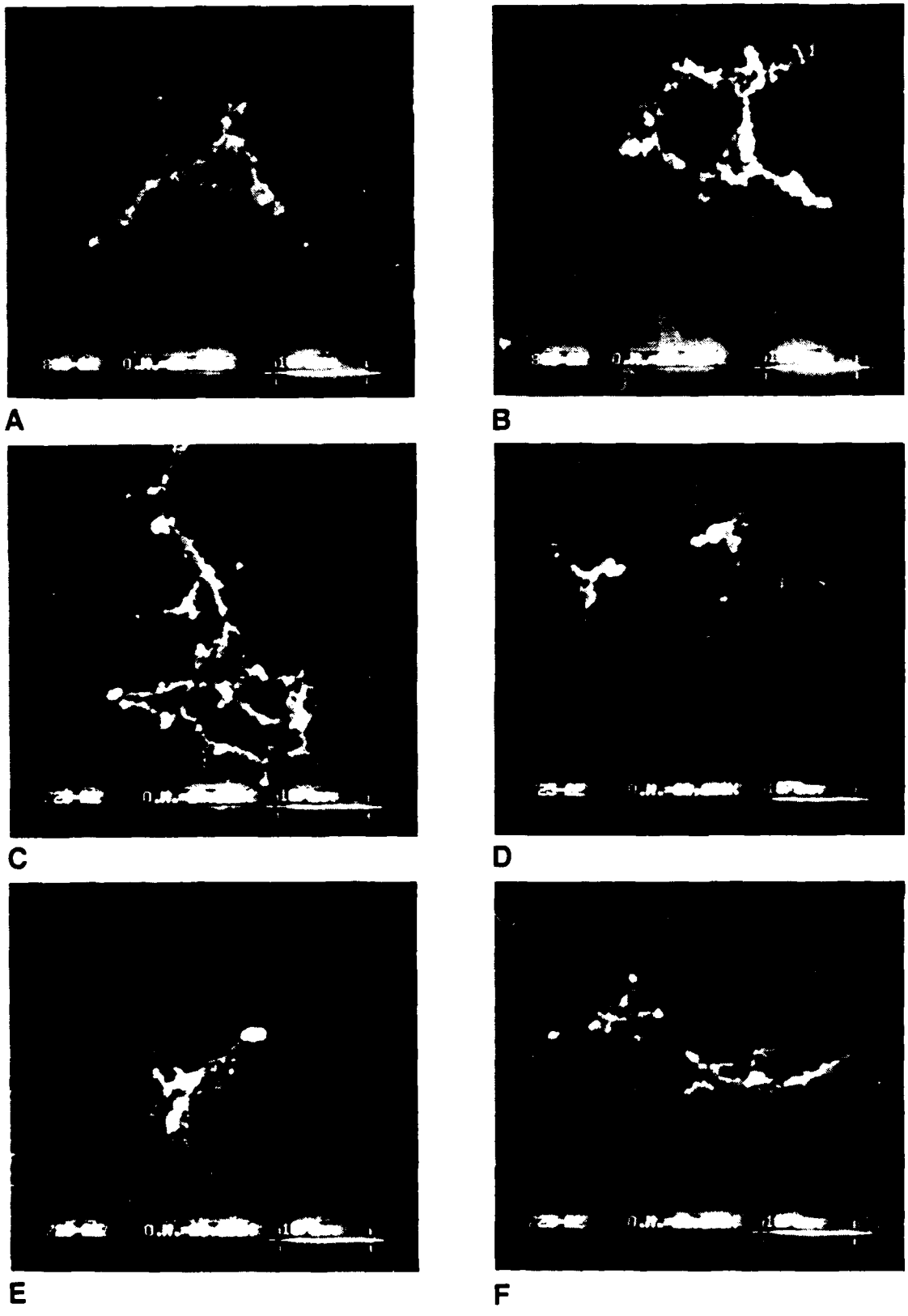

Figure A-12. Platinum aerosol: A,B — 0.01 atm.; C-F — 0.002 atm.

END
DATE
FILMED
4-88
DTIC